

Review

# Significance of Alloying Elements on the Mechanical Characteristics of Mg-Based Materials for Biomedical Applications

Sachin Kumar Sharma <sup>1</sup>, Kuldeep Kumar Saxena <sup>1</sup>, Vinayak Malik <sup>2,3</sup>, Kahtan A. Mohammed <sup>4</sup>,  
Chander Prakash <sup>5,6,\*</sup>, Dharam Buddhi <sup>7</sup> and Saurav Dixit <sup>7,8,\*</sup>

<sup>1</sup> Department of Mechanical Engineering, GLA University, Mathura 281406, India

<sup>2</sup> Department of Mechanical Engineering, KLS Gogte Institute of Technology, Belagavi 590008, India

<sup>3</sup> Department of Mechanical Engineering, Visvevaraya Technological University, Belagavi 590018, India

<sup>4</sup> Department of Medical Physics, Hilla University College, Babylon 51002, Iraq

<sup>5</sup> School of Mechanical Engineering, Lovely Professional University, Phagwara 144001, India

<sup>6</sup> Division of Research and Development, Lovely Professional University, Phagwara 144001, India

<sup>7</sup> Division of Research & Innovation, Uttaranchal University, Uttarakhand 248007, Dehradun, India

<sup>8</sup> Peter the Great St. Petersburg Polytechnic University, 195251 Saint Petersburg, Russia

\* Correspondence: chander.mecheng@gmail.com (C.P.); sauravambol@gmail.com (S.D.)

**Abstract:** Magnesium alloys are widely employed in various applications due to their high strength-to-weight ratio and superior mechanical properties as compared to unalloyed Magnesium. Alloying is considered an important way to enhance the strength of the metal matrix composite but it significantly influences the damping property of pure magnesium, while controlling the rate of corrosion for Mg-based material remains critical in the biological environment. Therefore, it is essential to reinforce the magnesium alloy with a suitable alloying element that improves the mechanical characteristics and resistance to corrosion of Mg-based material. Biocompatibility, biodegradability, lower stress shielding effect, bio-activeness, and non-toxicity are the important parameters for biomedical applications other than mechanical and corrosion properties. The development of various surface modifications is also considered a suitable approach to control the degradation rate of Mg-based materials, making lightweight Mg-based materials highly suitable for biomedical implants. This review article discusses the various binary and ternary Mg alloys, which are mostly composed of Al, Ca, Zn, Mn, and rare earth (RE) elements as well as various non-toxic elements which are Si, Bi, Ag, Ca, Zr, Zn, Mn, Sr, Li, Sn, etc. The effects of these alloying elements on the microstructure, the mechanical characteristics, and the corrosion properties of Mg-based materials were analyzed. The mechanical and corrosion behavior of Mg-based materials depends upon the percentage of elements and the number of alloying elements used in Mg. The outcomes suggested that ZEK100, WE43, and EW62 (Mg-6% Nd-2% Y-0.5% Zr) alloys are effectively used for biomedical applications, having preferable biodegradable, biocompatible, bioactive implant materials with a lower corrosion rate.

**Keywords:** alloying elements; corrosion properties; surface modifications; biocompatibility; EW42



**Citation:** Sharma, S.K.; Saxena, K.K.; Malik, V.; Mohammed, K.A.; Prakash, C.; Buddhi, D.; Dixit, S. Significance of Alloying Elements on the Mechanical Characteristics of Mg-Based Materials for Biomedical Applications. *Crystals* **2022**, *12*, 1138. <https://doi.org/10.3390/cryst12081138>

Academic Editor: Hongbin Bei

Received: 14 July 2022

Accepted: 28 July 2022

Published: 12 August 2022

**Publisher's Note:** MDPI stays neutral with regard to jurisdictional claims in published maps and institutional affiliations.



**Copyright:** © 2022 by the authors. Licensee MDPI, Basel, Switzerland. This article is an open access article distributed under the terms and conditions of the Creative Commons Attribution (CC BY) license (<https://creativecommons.org/licenses/by/4.0/>).

## 1. Introduction

Biomaterials include ceramics, polymers, metallic materials, and composites. In comparison to conventional metals, the biomaterials must have good tensile strength, and ductility, and be able to absorb the strain energy [1]. With these characteristics, orthopedic fixation devices and load-bearing applications including joint replacements, bone plates, screws, rods, wires, cardiovascular stents, and dental implants may be satisfied [2,3]. Traditional metals with strong biocompatibility, such as titanium, cobalt–chromium alloys, and stainless steel are employed as orthopedic implants in fracture treatment [3]. The drawback of these traditional metals was that they were not biodegradable; as a result, in

the majority of cases, a second surgery is required to remove the implants from the body after the tissue has healed. Implants typically remain in the body even after the fracture tissue has healed, which increases the risk of infection by allowing the implant material to corrode in a physiological environment [4]. The development of biodegradable implant materials with outstanding corrosion resistance to adapt to the physiological environment is regarded as the current research trend [5–7]. Materials that degrade naturally in vivo and in vitro are considered biodegradable. These materials totally disintegrate under the biological state, fulfilling the goal of assisting tissue healing without implant remains [2]. Through the process of dissolution, a non-toxic oxide is created, which is then harmlessly expelled through the urine. Because of this, the primary constituents of biodegradable materials are those metallic elements that are indigestible to humans and degrade at appropriate rates there.

The three types of biodegradable materials are pure metals, alloys, and metal matrix composites (MMCs) [6]. By selecting the appropriate reinforcement, metal matrix composites, which are biodegradable materials, can display characteristics including yield strength, tensile strength, and young's modulus, as well as corrosion resistance [8]. All components in biodegradable composites should be safe for human health and biodegradable. Magnesium, which is 33% lighter than aluminum and has a density of 1.74 to 2.0 g/cm<sup>3</sup>, is the lightest metal [7]. The density of the magnesium substance (1.84 g/cm<sup>3</sup>) is extremely similar to that of bone and it has a good strength-to-weight ratio. Due to their required biodegradation and mechanical characteristics, magnesium (Mg) alloys and their composites have been employed as standard implant materials and are being investigated as prospective alternatives [9]. The rate of degradation is extremely high under physiological conditions; as a result, the mechanical integrity of the implant may deteriorate prior to the full healing of the fractured bone tissue. Additionally, a significant amount of hydrogen gases is released, which postpones the healing of the fractured bone tissue [10]. This significant issue has led to the development of pure magnesium, magnesium alloys, and magnesium composites for use in biological applications.

The creation of degradable biomaterial based on magnesium (Mg) has recently attracted more attention. Although Mg is susceptible to corrosion, other physical characteristics, like its low density and high biocompatibility, have spurred major research and development in this field [10]. Several strategies have been used to overcome the problems of corrosion and the poor yield strength of pure magnesium, including the development of composites with suitable bioactive reinforcements, alloying, or surface modifications [10]. In order to maintain the mechanical properties of magnesium alloys and increase their surface biocompatibility for orthopedic applications, surface modification is primarily utilized to regulate the rate of degradation of magnesium alloys. Table 1 highlights the various surface modification approaches that were incorporated in Mg-based material composites.

**Table 1.** Surface Modification approaches related to Mg-based materials.

S.NO	Types of Surface Modification Approach	Modification Technique	Description	References
1	Chemical Modification	Acid Etching	<ol style="list-style-type: none"> <li>1. Removing the initial oxide layer and adding homogenous, and compact layers afterward that slowed the rate of degradation.</li> <li>2. The impact of acid etching as a pretreatment on the rate of degradation of the magnesium alloy AZ31 in SBF solutions analyzed by Munro et al.</li> <li>3. In comparison to unetched alloys, homogenous and dense films of Mg<sub>3</sub>(PO<sub>4</sub>)<sub>2</sub> layers were created on etched magnesium alloys, which significantly reduced the rate of degradation.</li> </ol>	[11]

Table 1. Cont.

S.NO	Types of Surface Modification Approach	Modification Technique	Description	References
2	Chemical Modification	Alkali Treatment	<ol style="list-style-type: none"> <li>1. After being submerged in an alkaline solution, a new passive layer made up of <math>MgCO_3</math>, <math>Mg(OH)_2</math>, and <math>MgO</math> is deposited on the surface of magnesium alloys that improving the corrosion resistance.</li> <li>2. Gu et al. analyzed the reduction in the degradation rate of Mg-based materials in SBF.</li> </ol>	[12]
3	Chemical Modification	Fluoride Treatment	<ol style="list-style-type: none"> <li>1. The most effective and practical method for surface modification of magnesium alloys at the moment is fluorination.</li> <li>2. In order to create samples of HF-coated magnesium alloys, Li et al. created screws and tensile specimens using magnesium alloys as substrates. Even after a month of immersion, <math>MgF_2</math>-coated samples maintained good mechanical characteristics due to a reduced rate of corrosion than bare samples.</li> </ol>	[13]
4	Physical Modification	Sol-gel Coating	<ol style="list-style-type: none"> <li>1. For a variety of metal substrates, including aluminum, steel, copper, magnesium, and their alloys, sol-gel coatings have been shown to have great chemical stability, excellent oxidation control, and increased corrosion resistance.</li> <li>2. To reduce the degree of degradation of magnesium alloys, Gaur et al. created a sol-gel silane coating using a combination of diethyl phosphate ethyl tri-ethoxy silane (DEPETES) and bis- [3- (tri-ethoxy silyl) propyl] tetra-sulfide (BTESPT).</li> <li>3. The samples with the sol-gel coating showed the greatest improvement in the rate of degradation.</li> </ol>	[14]
5	Physical Modification	Organosilane coatings	<ol style="list-style-type: none"> <li>1. For orthopedic purposes, it acts as a protective and biocompatible coating on Mg alloys.</li> <li>2. The hydrophobic Si-O-Si networks of organosilanes, minor galvanic reactions with Mg, increased adhesive strength, ease of chemical modification, and low cytotoxicity are only a few benefits of employing organosilanes as protective barrier coatings.</li> </ol>	[14]
6	Physical Modification	Calcium Phosphate Coating	<ol style="list-style-type: none"> <li>1. Different procedures have been used to deposit different forms of calcium phosphate coatings, such as hydroxyapatite (HA), fluorinated hydroxyapatite (FHA), and brushite on Mg substrates.</li> <li>2. One of the most effective methods discovered for covering the surface of orthopedic implants is calcium phosphate deposition.</li> <li>3. The corrosion resistance of Mg alloys covered with Ca-P was greatly increased compared to untreated magnesium alloys, according to Cao et al. who created a Ca-P coating on AZ31 alloys in SBF. Additionally, there were no harmful effects of the Ca-P coating on cells.</li> </ol>	[15]

Table 1. Cont.

S.NO	Types of Surface Modification Approach	Modification Technique	Description	References
7	Physical Modification	Superhydrophobic Coating	<ol style="list-style-type: none"> <li>1. One of the most current techniques to increase the corrosion resistance of Mg alloys is a superhydrophobic surface.</li> <li>2. A superhydrophobic surface with a 157.6° contact angle with water was created by Zhang et al. using AZ31 magnesium alloy. The superhydrophobic coatings considerably increased the corrosion resistance of the AZ31 alloy, according to the corrosion results.</li> <li>3. Superhydrophobic surfaces inhibit the contact between cells and implants, which limits the implant's capacity to stimulate bone repair and slows the rapid deterioration of magnesium alloys.</li> </ol>	[15]

Magnesium alloys degrade as a result of numerous redox processes, which the alloying elements can access. Practically, hydrogen gas and magnesium hydroxide are produced when magnesium decomposes in an aqueous solution as shown in Equation (1). Because of its capacity to remove hydrogen ions from an aqueous environment, the metal zinc is frequently utilized as an alloying agent. When this happens, the required reaction shown in Equation (2) takes place. The magnesium metal will take the zinc ions out of the water as shown in Equation (3) [16]. Due to hydrogen evaluation, the use of magnesium alloys as implants is not desirable. As seen from the aforementioned reactions, the rapid corrosion rate of magnesium metal produces hydrogen gas with an aqueous solution. It is advised to slow down the corrosion of Mg alloy to resolve the degradation rate of Mg.



In biomedical applications proposed for the development of orthopedic implants (joint and hip replacement, prosthesis, etc.) and temporary implants, the use of metallic metals has dramatically increased (wires, plates, rods, pins, screws, etc.) [16]. Magnesium has been utilized for more than a century as a biodegradable implant material in vivo and in vitro. Comparing magnesium composites to other metallic metal composites, they had high biocompatibility. Magnesium is a vital component of human life and is the fourth-most prevalent element in the human body [16,17]. Table 2 compares the value of Mg composites versus Co-Cr alloy, titanium alloys, and stainless steel as implant materials. [18]. It was suggested that the commercially available AZ91D magnesium alloy be used as a matrix in magnesium composites for orthopedic applications after the metallic reaction of the alloy was studied in vivo and in vitro. Magnesium material corrodes quickly and emits hydrogen (H<sub>2</sub>) gas, which was observed in a few experiments. Modern techniques were created to slow the pace of corrosion of Mg-based material and cure tissue damage without requiring additional surgery to remove the implanted material [15]. The majority of researchers are working to produce implants for orthopedic applications and cardiovascular stents using biodegradable Mg-based materials [12–16]. Table 3 identified the mechanical properties of Mg alloy and other metallic implant materials.

**Table 2.** Comparison of Mg alloy with other metallic implants.

S.NO	Material	Benefits	Drawbacks	Applications
1	Co-Cr alloy	1. Provides good resistance to fatigue, wear, and corrosion. 2. Provides high strength. 3. Long-span biocompatibility.	1. Very expensive. 2. Machining is difficult.	1. Bone implantation (wires and plates). 2. Hip replacement.
2	Ti alloy	1. Enables good corrosion resistance and has low young's modulus with suitable biocompatibility. 2. High strength than 316L stainless steel.	1. High wear rate. 2. Very expensive.	1. Fracture fixation. 2. Total joint replacement.
3	316L Stainless steel	1. Easily available, high toughness, suitable biocompatibility, inexpensive, and good fabrication characteristics.	1. High corrosion, and wear rate, high-stress shielding effect.	1. Bone implantation.
4	Mg-alloy	1. Biocompatible, bioresorbable, biodegradable, and bio-active. 2. Elastic modulus resembling human bone. 3. Low-stress shielding effect and lightweight.	1. High H <sub>2</sub> evolution during degradation	1. Bone implantation, screws, and plates.

**Table 3.** Mechanical properties of Mg alloys and other metallic implants.

S.NO	Material Property	Human Bone	Mg Alloys	Ti Alloys	Co-Cr Alloys	Stainless Steels
1	Density (g/cm <sup>3</sup> )	1.8–2.1	1.74–2.00	4.4–4.5	8.3–9.2	7.9–8.1
2	Yield Strength (MPa)	30–114.3	20–200	896–1034	448–1606	221–1213
3	Compressive Strength (MPa)	164–240	55–130	N/A	N/A	N/A
4	Young's Modulus (GPa)	3–23	41–45	110–117	210–232	189–205
5	Fracture toughness (MPa/m <sup>1/2</sup> )	3–7	15–40	55–115	50–200	NA
6	Tensile Strength (MPa)	70–150	86–280	760–1140	655–1896	586–1351
7	Elongation (%)	1.07–2.10	12–21	12	N/A	N/A

It has been suggested that graphene is a wonder material with great charge carrier mobility, large surface area, and exceptional mechanical characteristics. Additionally, graphene's long-extend  $\pi$ -conjugation is a crucial photocatalytic characteristic that enables a variety of biosensor activities. Due to the broad application of nanographene, recent developments in biomedical applications and materials science, such as scaffold, cancer nanotechnology, tissue manufacturing, drug delivery, and antimicrobial activities, have been incorporated [17]. Graphene-assembly nano biosensors are now one of the top choices among researchers since they are safe to use, cost-effective, less time-consuming, and most importantly used for the daily assessment of glucose levels [18]. The use of nanoparticles (NP) to eradicate bacteria that are free-floating and those that form biofilms is one of their important applications in healthcare [19]. It has been demonstrated that a number of nanoparticles, including CuO, Fe<sub>3</sub>O<sub>4</sub>, ZnO, MgO, Al<sub>2</sub>O<sub>3</sub>, etc. can accomplish this property with varying levels of functionality. Using nanocomposite (NC) materials to

remove germs is a more sophisticated and effective technique to destroy bacterial biofilms. Materials similar to chitosan and graphene can also be utilized to make several forms of the nanocomposite, in addition to different metal oxides [20]. The capacity of nanoparticles and nanocomposites to avoid the issue of bacterial resistance is one of their main advantages over antibiotics. In biomedical applications such as hip joints, cardiovascular stents, bone fixation, and dental implants, the Mg-based bio-composite is used [20].

Biodegradable metals (BMs) slowly deteriorate in living tissue by generating corrosion products when they are in contact with the body's physiological conditions [21]. Biodegradable implants that completely dissolve with no implant material left in the surrounding tissues help in the recovery and repairing of tissue bone. Three kinds of BMs—Fe-based, Mg-based, and Zn-based BMs—have undergone substantial research in recent years. Mg-based materials have undergone the most clinical testing among the three BMs. While Fe-based BMs show slower and less complete in vivo breakdown, Mg-based BMs often exhibit higher degradation rates, which might not match the bone tissue's healing times. Due to their intermediate degradation rates, which fall between those of Mg- and Fe-based BMs, Zn-based BMs are now regarded as a new class of BMs [22]. Hussein et al. analyzed the corrosion behavior of eggshell-reinforced Mg and Mg-Zr alloy and observed that the eggshell has the potential to be exploited as efficient green reinforcing particles in the creation of Mg and Mg-Zr-based composites, with better in vitro corrosion characteristics for biomedical applications [23].

By advancing green chemistry to create “Greenery Nanoscience and Nanotechnology,” nanoscience ensures a promising future. The “Green Chemistry” technique, which is attributed to the bigger pore volume and long-range surface area of gold nanoparticles, is the one and only outstanding method authenticated for the enhancement and execution of chemically assisted processes in order to limit the usage of toxic compounds [24]. Currently, low-cost natural and waste products have been treated with hazardous chemicals to produce value-added nanomaterials with wide applications, proposing an affordable and environmentally friendly solution to environmental problems.

Magnesium-based alloys had received a lot of attention as potential biodegradable implant materials in biomedical applications [1–3]. For orthopedic applications, a new generation of bioactive, biocompatible, and biodegradable metallic materials has recently been discovered. Due to its great biocompatibility and adequate strength, pure magnesium, magnesium alloys, and magnesium alloy-based composites are widely used in biomedical applications [25]. In a biological environment, pure magnesium and magnesium alloys can corrode too quickly and lose their characteristics before bone healing. The new era of composites made of magnesium can meet the needs of orthopedic applications. Magnesium-based composites are biomaterials that can create suitable mechanical properties under a biological environment, such as ultimate tensile strength, elastic modulus, ductility, and resistance to corrosion [26]. The matrix materials used in magnesium-based composites, such as Mg-Zn, Mg-Al, Mg-Ca, and Mg-REE alloy, are biomedical magnesium alloys [27]. The usage of Mg alloys as biomaterials enriches the growth of magnesium alloys in biodegradable metallic implants that showcase the influence of alloying elements such as Al, Zn, Li, Mn, Zr, Ca, Sr, and rare earth elements on resistance to corrosion, mechanical characteristics, and biocompatibility of Magnesium alloys. Ce, Gd, yttrium, lanthanum, erbium, and neodymium are the somewhat-rare earth elements employed as an alloying element in Mg alloys [3]. This detailed review includes the classification of alloying elements and their significance in influencing the mechanical characteristics of Mg-based material for biomedical applications.

## 2. Alloying Elements Suitable for Biomedical Application

Magnesium alloys are widely used in many applications, such as aerospace, automotive, defense, biomedical, etc., due to their excellent mechanical properties and high corrosion resistance compared to unalloyed magnesium [4]. Magnesium as-cast has a high rate of deterioration and weak strength. As a result, the material characteristics can be

improved by using appropriate alloying and processing methods. Chemically active magnesium reacts with alloying substances to produce intermetallic compounds [27]. These intermetallic phases, which have been found in magnesium alloys, are what affect the microstructure, which in turn affects the material properties. The alloying elements directly strengthen the mechanical characteristics by precipitation hardening, grain refining, and solid solution strengthening [28]. The two main factors affecting solubility are the element's valence and atomic size relative to magnesium. Magnesium's HCP (hexagonal close-packed) structure and atomic diameter of 0.320 nm ensure the creation of solid solutions including a variety of elements [26–29]. Magnesium alloys are found in binary, ternary, and other forms [5,6]. However, it is an essential prerequisite to identify the suitable alloying element to improve the mechanical properties and adopt high corrosion resistance in magnesium alloys that involve suitable biocompatibility of the implant through non-toxic properties [7]. Table 4 briefly mentions the most popular alloying elements and their effects on magnesium alloy. The number of alloying elements and the percentage of the alloying element can be used to determine the influence of each of these alloying elements. The influence of various alloying elements depends on the percentage of elements used in Mg along with the amount of alloying elements discussed below [9].

**Table 4.** Role of alloying elements in improving the mechanical properties.

S.NO	Elements	Improvement in Mechanical Properties
1	Calcium	Improvement in grain refinement and enhances the strength of the MMCs
2	Lithium	Improvement in ductility and reduction in strength
3	Zinc	Addition of zinc up to 5 wt.%. enhances the strength of the composite
4	Strontium	With 3 wt.% of strontium, the reduction in elongation provides an improvement in strength and enhances the refinement of the grain size
5	Manganese	Addition of Manganese improves the grain refinement and tensile strength
6	Tin	Tensile and compressive strength gets improved by tin addition
7	Zirconium	Zirconium provides high damping strength, tensile strength, and involves high ductility
8	Aluminum	Aluminum improves the hardness and tensile strength
9	Titanium	Improvement in elongation is observed with titanium
10	Copper	Reduction in ductility is observed with the addition of copper
11	Silicon	Enhancement in fluidity is observed with the addition of silicon
12	Iron	Not suitable for corrosion resistance
13	Neodymium	Improvement in strength is observed with neodymium
14	Molybdenum	Improvement in Young's modulus, hardness, and elongation
15	Cerium	Reduction in yield strength is observed

### 2.1. Calcium (Ca)

The alloying element calcium is 1.34% soluble in magnesium in the equilibrium condition [10]. The addition of calcium in magnesium improves the thermal and mechanical properties of Mg alloy [30]. The addition of calcium in Mg enhances the rollability of magnesium sheets with less than 0.3 wt.% of calcium but with an increase in the percentage of calcium, the magnesium sheets will develop a crack over the surface during welding [31]. For biomedical implantation, 1 wt.% of calcium in Mg provides good accountability for biocompatibility [32]. The corrosion resistance in Mg alloys is very low around 1.34 wt.% of calcium in Mg [33].

## 2.2. Aluminum (Al)

Aluminum is the most commonly used alloying element in magnesium which increases its strength to a greater extent, i.e., by 180 mpa [19,20]. The solubility of aluminum in Mg is greatly influenced by the temperature of around 12 wt.% of aluminum in Mg [34]. The corrosion rate of an alloy is improved via cathodic reaction by the addition of more than 3 wt.% of aluminum [35]. Aluminum enhances the susceptibility to the stresses in corrosion cracking in alloys with the presence of  $\beta$ -phases in the composite [36–39].

## 2.3. Copper (Cu)

The alloying element copper has low solubility in Mg as a result of it having a negative effect on corrosion resistance and forming the  $Mg_2Cu$  phase with pure Mg [40]. Copper has a tolerance limit in pure Mg of around 0.1 wt.% but the presence of aluminum and manganese in the alloys reduces the tolerance limit to 0.01 wt.% [41]. The addition of copper in Mg alloy causes a reduction in elongation along with an increase in the strength of the alloy [41].

## 2.4. Manganese (Mn)

The alloying element manganese has low solubility in Mg around 2.5 wt.% but the addition of manganese in Mg alloy up to 5 wt.% entails no change in corrosion rate [42]. Therefore, manganese is advisable to be used simultaneously along with other alloys such as copper, and aluminum [43]. Manganese is regarded as an essential element in the body that is required for a healthy bone–tissue framework [44]. Manganese's role helps in preventing osteoporosis and promotes the formation and metabolism of bone [45]. In the Mg alloys, the effect of iron is reduced, with manganese sticking to iron, as a result of which the iron-to-manganese ratio reaches the maximum value of 0.032, as, beyond this limit, the corrosion resistance is extremely low [46]. A recent study focused on the encapsulation of iron by manganese in an aluminum-based alloy of Mg which extremely influences the sequestration of iron without the presence of aluminum [47].

## 2.5. Bismuth (Bi)

The alloying element bismuth promotes the reactions at anode and cathode which promotes the increased corrosion rate of Mg [48]. However, it is beneficial for improving the tensile strength of the magnesium by preventing the sliding of grain boundaries around the surface [49].

## 2.6. Iron (Fe)

The alloying element iron, up to 0.005 wt.%, is highly accountable for controlling the corrosion rate in pure Mg, but beyond that limit, it has negative effects on the magnesium-based alloy composite [50–53]. It is found in the form of impurities in Mg alloys. Iron has low solubility at 0.001 wt.% in Mg which keeps magnesium in its pure state [51]. Therefore, the addition of a limited amount of Fe in Mg can be beneficial for improving corrosion resistance [52].

## 2.7. Lithium (Li)

The alloying element lithium has an extremely low density of around 0.54 g/cc but is found to have high solubility in Mg [53]. The experimental study of various researchers suggested that lithium influences the ductility of Mg by forming suitable changes in the crystal structures [54]. With the continuous addition of lithium, the Mg is found to be worn out [55,56]. Lithium increases the intercellular concentration of Mg alloy by allowing the formation of an intercellular binding site with Mg [57].

## 2.8. Molybdenum (Mo)

The alloying element molybdenum is highly insoluble in Mg; hence, it does not form an alloy with Mg [56]. The study suggested that the addition of 0.1 wt.% of Mo in Mg

alloy (AZ91E) at a micro-level improves the corrosion resistance and current density of the alloy [57]. The addition of molybdenum in Mg alloy promotes the enhancement in hardness, elastic modulus, and elongation of alloy [58].

### 2.9. Holmium (Ho)

There have been few experimental studies done to analyze the influence of holmium in Mg alloys, which suggested that Holmium reduces the corrosion resistance with the addition of 0.24 wt.% and 0.44 wt.% of holmium to Mg-Al alloy (AZ91D) [59,60]. The reduction in resistance to corrosion leads to the formation of intermetallic compounds of holmium along with a reduction in the formation of  $\beta$ -phase ( $Mg_{17}Al_{12}$ ) [61]. The research study suggested that holmium in Mg-Al alloy slightly reduces the cathodic reaction rate and lowers the mass loss rate up to 11 times that of Mg-Al alloy which decreases the strength of the base alloy [61]. The addition of holmium provides uniform dispersion and suitable compaction to the corrosion layer with the presence of a large amount of Al in Mg [62].

### 2.10. Erbium (Er)

There hasn't much research work been accomplished with the addition of alloying element erbium in Mg. The study suggested that the reduction in corrosion rate is observed at 2 to 3wt.% of erbium in Mg-Al alloy as compared to AM60 alloy in a buffer solution of borate [63].

### 2.11. Gadolinium (Gd)

The alloying element gadolinium has a high solubility in Mg with more than 10 wt.%, and the addition of gadolinium forms the Al-Mn-Gd and  $Al_2Gd$  phases which diminishes the  $\beta$ -phase ( $Mg_{17}Al_{12}$ ) and causes a reduction of aluminum in Mg-Al alloy [49]. The formation of Al-Mn-Gd and  $Al_2Gd$  phases reduce the rate of cathode reaction [64–66]. The gadolinium in Mg-Al alloy forms the heterogeneous mixture and reduces the aluminum concentration which made Mg-Al alloy complicated [51]. Therefore, the corrosion rate is increased in Mg-Al alloy via the addition of gadolinium [52]. Hence, gadolinium has a negative effect on the corrosion rate of the Mg-Al alloy.

### 2.12. Cerium (Ce)

The alloying element cerium is a rare earth element that enhances corrosion resistance, wear resistance, and thermal strength in Mg [67,68]. With 0.2 wt.% of cerium in Mg, the appropriate elongation is obtained [54]. The cerium improves the corrosion rate in binary Mg-Ce alloy with the presence of the  $Mg_{12}Ce$  phase which improves the cathodic reaction rate [69–71]. The wrought Mg alloy prevents the formation of  $Al_xRE_y$  compound (the combination of Ce and Al) that reduces the ductility of Mg alloy. However, cerium improves the surface layer by stabilizing the magnesium hydroxides [71].

### 2.13. Lanthanum (La)

The alloying element lanthanum is highly soluble in Mg between 3 to 5 wt.%, but beyond the solubility limit, a reduction in corrosion resistance is observed due to the presence of the  $Mg_{12}La$  phase, which enhances the cathodic reaction rate [72]. The addition of lanthanum to Mg-Al alloy enables a change in the microstructure of the Mg-Al alloy which produces the needle-shaped structure of the Al-La phase [73]. It remodels the  $\beta$ -phase ( $Mg_{17}Al_{12}$ ) into a fine continuous polygon shape [73]. A research study suggested that the increased corrosion resistance of Mg alloy (AZ91) is observed at 0.5 wt.% of lanthanum in 3.5 wt.% of NaCl due to the refinement in grain size and higher shielding of corrosion film [59]. However, adding lanthanum in the Mg-Al alloy beyond the solubility limit increases the corrosion rate due to Al-La phase formation [74].

#### 2.14. Neodymium (Nd)

The alloying element neodymium allows the formation of the  $Mg_3Nd$  phase in Mg-Nd alloy, which reduced the corrosion resistance due to it increasing the cathodic reaction rate in Mg by  $Mg_3Nd$  phase [75]. The addition of neodymium in Mg lowers the corrosion rate as compared to Lanthanum and Ce [76]. The reduction in galvanic coupling in neodymium is the main reason behind the increase in resistance to corrosion of Mg-Al alloy [76]. However, neodymium provides a protective oxide layer over the Mg-Al alloy surface, comprising Mg and rare earth metals, which improves the resistance to corrosion.

#### 2.15. Strontium (Sr)

The alloying element strontium is regarded as an essential element in the body that enables the development of osteoblasts by hindering bone resorption [77]. Like silver, strontium is also most suitable along with rare earth elements and is not soluble in Mg [77]. The addition of strontium in Mg alloy forms the  $Mg_{17}Sr_2$  phase along with the refinement of grain size [77]. The strontium in Mg led to a high corrosion rate due to an increase in corrosion potentials [78]. Strontium is regarded as a bone-seeking element that improves the remodeling and regeneration of injured/damaged bone and bone formation. The promoting action of strontium on calcium uptake into the bone at moderate strontium supplementation and the rachitogenic action of strontium at higher dietary strontium levels are improved. Sr refines the grain size in Mg alloys and has a high Mg alloying efficiency [78]. The amount of intermetallic phase increases with increasing Sr content in the Mg-Sr alloy, which is made up of  $Mg_{17}Sr_2$  and  $\alpha$ -Mg as the primary phases. Additionally, Sr promotes biocompatibility, bone growth, and compressive strength. However, Sr concentrations beyond 2% in Mg-Zr-Sr alloys cause the intermetallic phase  $Mg_{17}Sr_2$  to precipitate at the grain boundary, which lowers corrosion resistance [76–78]. Therefore, the Sr level should be below 2% pre-osteoblastic cell replication is accelerated by Sr, which also promotes bone development [62].

#### 2.16. Zirconium (Zr)

The alloying element zirconium is mostly used along with rare earth elements or along with radioactive elements which act as grain refiner around the grain boundary [79]. Zirconium has the strong capability to form compounds with Manganese and Aluminum [64]. Hence, zirconium is not a suitable alloying element along with manganese and aluminum. During the melting of Mg, zirconium reacts with hydrogen, oxygen, carbon, and iron to form a stable compound [80,81]. Zirconium is not soluble in Mg, due to which no intermetallic compounds are formed [82]. The research study suggested that zirconium is a prerequisite in reducing the corrosion rate and enabling the reactions at the anode to have negative effects on the surface film [66]. Therefore, zirconium is most suitable for reducing the harmful corrosion effect on Mg alloy [67].

#### 2.17. Yttrium (Y)

The alloying element yttrium is soluble in Mg around 2 to 18 wt.% [68]. The addition of yttrium promotes the increase in corrosion rate with an increase in the formation of the  $Mg_{24}Y_5$  phase which led to a rise in the rate of cathodic reaction [68]. A research study suggested that about 0 to 0.8 wt.% of yttrium in Mg alloy (AZ91) improved the corrosion resistance properties which led to a reduction in  $\beta$ -phase and improved the homogeneous dispersion of  $\beta$ -phase ( $Mg_{17}Al_{12}$ ) [69]. The microstructural characterization of yttrium in Mg shows the refinement in grain size that reduces the corrosion rate [70]. The high solubility of yttrium made it suitable in commercial WE54 and WE43 alloys [71].

#### 2.18. Silver (Ag)

The alloying element silver is most appropriately used with rare earth elements in Mg. The addition of 0.5 wt.% of Ag has significant tolerance but beyond the limit mass loss had increased monotonously [72]. The corrosion behavior of silver resembles the corrosion

behavior of calcium. Less than 2 wt.% of silver in Mg promotes the improvement in the strength of Mg-RE-Zr alloy [72]. The Silver in Mg alloy (AZ91) improves the hardness of the alloy without affecting the resistance to corrosion of alloy due to the contact of  $\beta$ -Mg<sub>17</sub>Al<sub>12</sub> phase and Ag [73].

#### 2.19. Tin (Sn)

The alloying element tin is non-toxic but tin salts can be carcinogenic [74]. The addition of tin is beneficial for human health but its functionality has not been defined yet [74]. Tin in Mg forms the Mg<sub>2</sub>Sn phase which led to the refinement in grain boundaries with an increase in the volume of the Mg<sub>2</sub>Sn phase with the increasing quantity of tin [74].

#### 2.20. Zinc (Zn)

The alloying element zinc in Mg alloy improved the weldability by alloying along with thorium (Radioactive element). The addition of zinc along with aluminum is most effective in improving the strength of the alloy [75]. The zinc in the Mg alloy overcomes the impurities of nickel and iron to enhance the corrosion resistance of the alloy [76]. For 2.5 wt.% of zinc in Mg alloy, the alloy forms the suitable tolerance limit but the corrosion rate increases by increasing the percentage of zinc from 1 wt.% onwards along with inclination towards corrosion cracking [77]. Zinc is the most important element for nutritional purposes in the body with around 85% of zinc used by bone and muscles [76]. The 6.2 wt.% of zinc has a high solubility in Mg alloy [77]. Although zinc alloys resemble the mechanical characteristics of Mg alloys, the higher value of elastic modulus of zinc alloys produces a negative effect on bone recovery and tissue regeneration during the healing process in biomedical applications, because zinc alloys are subject to non-uniform load transfer during bone implantation [78].

### 3. Classification of Mg Alloy and Influence of Alloying Element on Various Mg Alloys

The alloying element such as aluminum, titanium, and magnesium are widely used in technologies and are the most suitable substitute for steel employed in structural applications [3]. Mg alloys have the lightest structure of all the non-ferrous element metals [5]. Therefore, one research study suggested that the usage of Mg-based alloys has increased in biomedical and structural applications [6]. During the formation of Mg-based alloys in biomedical applications, biocompatibility is the most important factor that governed the effectiveness of bone-implant and tissue regeneration without any toxic effects on living tissues [79]. The Mg-based alloys can be classified as wrought and cast magnesium alloys based on the processing approaches required for engineering applications and research and development perspectives [80]. The Mg alloys obtained via die and various casting approaches are referred to as-cast alloys [81]. The research study suggested that cast Mg alloys can be employed in limited areas where reasonable mechanical properties are required and are commonly used in industrial and commercial applications [6]. The wrought Mg alloys are obtained via secondary manufacturing processes such as Rolling, Equal-Channel Angular Pressing (ECAP), Extrusion, and Severe Plastic Deformation (SPD), while SPD is the most suitable approach for a reduction in grain size in microstructure characterization [82]. The researcher's approach suggested that the wrought Mg alloys had remarkable mechanical properties as compared to cast Mg alloys [81]. The wrought alloys enable the homogenous composition of alloy along with grain refinement having no pores on the surface of the alloy [80]. The classification of various magnesium alloys was illustrated in Figure 1. The Mg alloy can be binary, ternary, and quaternary subject to the presence of several phases and alloying elements in the alloy [83]. A comparative study of the mechanical properties of various alloys is illustrated in Table 5.

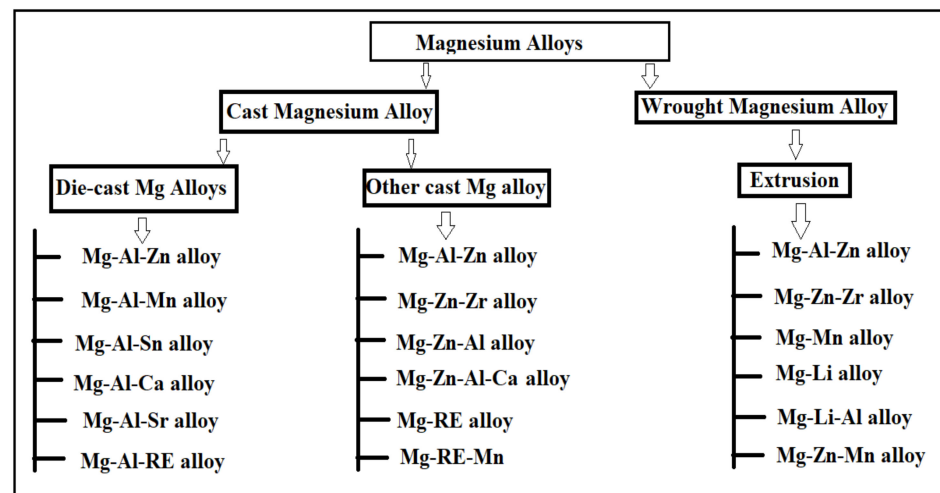


Figure 1. Classification of various Mg-based alloys.

Table 5. Comparative study of mechanical properties of alloying element in Mg alloy.

Composition by wt. %	Methodology	Post-Treatment	Yield Strength (MPa)	Ultimate Tensile Strength (MPa)	Elongation (%)
Mg-3Al	Casting process	Solid solution treatment	149	245	2.9
Mg-2Ca	Rapid solidification process	-	-	390	7.4
Mg-Zn-0.8Sr	Zone solidification process	Heat treatment	118	205	11.9
LAE442	Casting process	-	150	250	17.5
AZ31	Casting process	-	-	270	14.8
Mg-2Sr	Casting process	Hot rolling	145	275	-
Mg-6Zn	Casting process	Heat treatment and extrusion	285	180	20
Mg-Y-RE-Zr	Powder metallurgy process	-	255	270	10.5
Mg-5.0Y-7.0Gd-1.3Nd-0.5Zr	Casting process	Extrusion	160	230	25.5
Mg-Y	Casting process	-	155	245	14.5
Mg-5.0Y-7.0Gd-1.3Nd-0.5Zr	Casting process	Extrusion & aging	190	245	21.5
Mg-3Sn-0.5Mn	Casting process	Extrusion	145	245	12
ZW21	Casting process	Squeezing	195	275	18
WE43	Casting process	Heat treatment	165	225	45
WE43	Casting process	Extrusion and heat treatment	195	285	11

Table 5. Cont.

Composition by wt.%	Methodology	Post-Treatment	Yield Strength (MPa)	Ultimate Tensile Strength (MPa)	Elongation (%)
Mg-1Zn	Casting process	-	90	185	10
Mg-Zn-Mn	Zone solidification process	Extrusion	250	285	21.5
Mg-Y-Zn	Casting process	Extrusion	-	255–275	17–21
Mg-Zn-1Sr	Zone solidification process	Heat treatment	125	250	14
AZ31	Casting process	-	100-190	250–280	14–20
WE43A	Casting process	Heat treatment	160	255	-

### 3.1. Mg-Al Based Alloys

When aluminum is dissolved in Mg, the formation of the  $\alpha$ -Mg phase and  $\text{Y-Mg}_{17}\text{Al}_{12}$  phases (eutectic ternary phases) occur which enhances the solid-solution strength [84]. Mg-Al alloy is the most predominantly used Mg alloy due to its high specific stiffness, high specific strength, good electromagnetic shielding, good vibration properties, good anti-radiation properties, and other characteristics. Thus, Mg-Al alloys, also referred to as the “green engineering materials of the twenty-first century,” have a wide range of potential applications in automobiles, electrical equipment, electronics, transportation, aviators, and biomedical application fields [84]. Mg-Al alloys are vitally used in bone implantation with good tissue healing and low-stress shielding effect on the implant. The literature suggests that the mechanical properties (compressive and tensile strength) of Mg-Al binary alloys with Al content that exceeded the solubility limit significantly increased. Furthermore, the addition of more than 6 wt.% of Ca in the Mg-Al alloy significantly improves the tensile and compressive strength of the Mg-Al alloy. The Mg-Al-based alloys have superior castability with average mechanical properties [85]. The most commonly used alloying element in Mg-Al alloys is zinc and manganese with a concentration of around 1 wt.% [84]. The Mg-Al-based alloys usually have AM, AE, and AZ series which are biodegradable in nature that involves AM60, AZ31, AZ81, AZ61, and AZ91 alloys [85]. The AZ31 alloy indicates A as aluminum and Z as zinc and number 3 and 1 indicate 3% of Aluminum and 1% of zinc, respectively [79]. The AM series comprises various alloys involving Mg inclusive of aluminum and manganese such as AM30, AM40, AM50, and AM60, etc. [86]. The AM-based alloy has higher mechanical properties and suitable extrudability in comparison with AZ alloys having an absence of eutectic ternary phases containing zinc [84]. The Mg-based alloys involve the addition of zinc to provide strength to solute particles, but Manganese is added to improve the anti-corrosion properties of the alloy by eliminating the patches of iron from the alloy [87]. The Mg-Al-based alloys have negligible age-hardening due to the formation of the  $\beta$ - $\text{Mg}_{17}\text{Al}_{12}$  phase [84]. About 70% of the grains identified in microstructures are recrystallized to an average grain size of 1.2  $\mu\text{m}$  [85–88]. The various Mg-Al alloys along with the effect of the alloying element are illustrated in the below section.

#### 3.1.1. AZ Alloy Series

The addition of alloying element lithium in AZ31 alloy has optimized the microstructure of the alloy, as lithium enables the formation of a cross and non-basal slip [89]. Lithium is highly soluble in AZ31 alloy, allowing the alteration in lattice parameters of a solid solution of magnesium [89]. For an increase in the amount of lithium in AZ31 alloy, the random distribution of grains around the boundaries and a large reduction in basal structure intensity are obtained [90]. Additionally, lithium also promotes an enhancement in ductility

and reduction in anisotropy of AZ31 alloy due to the recrystallization of grains around the boundary [89]. The tensile strength of the alloy remains the same with the addition of lithium [90]. The research study by Meng et al. suggested that a high value of elongation and tensile strength were found in Mg-1Al-1Zn-8Li, these being 9.2% and 233.38 MPa, respectively [91,92]. The addition of tin in Mg-Al alloy enhanced the compressive and tensile properties of Mg-Al-based alloy composite due to a reduction in the stacking energy in the alloy [93]. Wu et al. suggested that the grain size in AZ91 is refined via the addition of tin in hot extrusion due to the restriction in the formation of Mg<sub>2</sub>Sn precipitates around the grain boundary [94]. The rare earth elements in Mg-Al alloys allow the formation of thermally stable phase (Mg, Al)<sub>x</sub>RE<sub>y</sub> as a result of that the enhancement in the mechanical properties of wrought Mg alloys that occurs [94]. The microstructure of the alloy AE44 (Mg-4.0Al-4.1RE-0.3Mn, wt.%) produced here mostly consists of α-Mg grains and Al<sub>11</sub>RE<sub>3</sub> intermetallic phase at grain boundaries. Additionally, TEM images depict a lamellar phase with primarily Al<sub>11</sub>Ce<sub>3</sub> indicated in Figure 2 [95]. The TEM also found trace phases. Both the lamellar phase and the feather-like phase contain La, Ce, Nd, and Al with an Al/RE ratio near 11:3, according to the results of the EDX micro-analysis, and the XRD pattern further demonstrates that the inter-metallics are a part of the Al<sub>11</sub>RE<sub>3</sub> phase (Al<sub>11</sub>Ce<sub>3</sub>) [95]. Pan et al. analyzed the effects of yttrium on the microstructure and mechanical properties of AZ31 alloy [68]. At 0.5 wt.% of yttrium in Mg-Al alloy, high yield strength of around 209 MPa was observed due to the formation of the Al<sub>2</sub>Y phase [71]. At 0.9 wt.% of yttrium in AZ31, the optimal mechanical properties were obtained, i.e., YS (yield strength), UTS (ultimate tensile strength), and elongation (%) are 258.9 MPa, 371.9 MPa, and 7.33% due to refinement in grain size of the Al<sub>2</sub>Y phase [71]. The coarse and brittle Al<sub>2</sub>Y phase was obtained at 1.4 wt.% of yttrium in AZ31 which causes a reduction in the tensile strength of the alloy [71].

The addition of 0.12 wt.% Mn as an alloying element in the Mg-Al alloy eventually replaces the Al-Fe phase with the Al<sub>8</sub>Mn<sub>5</sub> phase. Figure 3a illustrates the XRD image of the Mg-3Al-xMn alloy depicting the presence of Al<sub>8</sub>Mn<sub>5</sub> and MgF<sub>2</sub> in the alloying composition (Mg-3Al-0.12Mn and Mg-3Al-0.21Mn), respectively. During the creation of the samples, the MgF<sub>2</sub> phase was produced by the reaction of the Mg melt with the safety of SF<sub>6</sub> gas. The potentiodynamic polarization curve for each sample of Mg-3Al-xMn was analyzed in a 3.5 wt.% of NaCl solution depicted in Figure 3b [96]. The cathodic branches of the polarization curves of the alloys with Mn added were smaller than those of the alloy with Mg-3Al, indicating a decrease in the cathodic hydrogen reaction. The anodic polarization curves of the Mg-3Al-0.36Mn and Mg-3Al-0.45Mn alloys showed clear passivation behavior, although the curves of other alloys had active dissolving features. Additionally, the breakdown potential (E<sub>b</sub>) of the passive film (depicted by the black arrow) was obtained. The current density steadily reduced as Mn addition increased, and was observed to be the lowest for Mg-3Al-0.45Mn alloy. The higher value of (E<sub>b</sub>-E<sub>corr</sub>) indicated a passivation film that was more stable [96]. The breakdown potential for Mg-3Al-0.45Mn (94 mV) was observed to be higher than the Mg-3Al-0.36Mn alloy, suggesting that the passive film was more stable, indicating the lower propensity to develop localized corrosion. Therefore, corrosion resistance was observed to be enhanced with the addition of Mn to Mg-Al alloy.

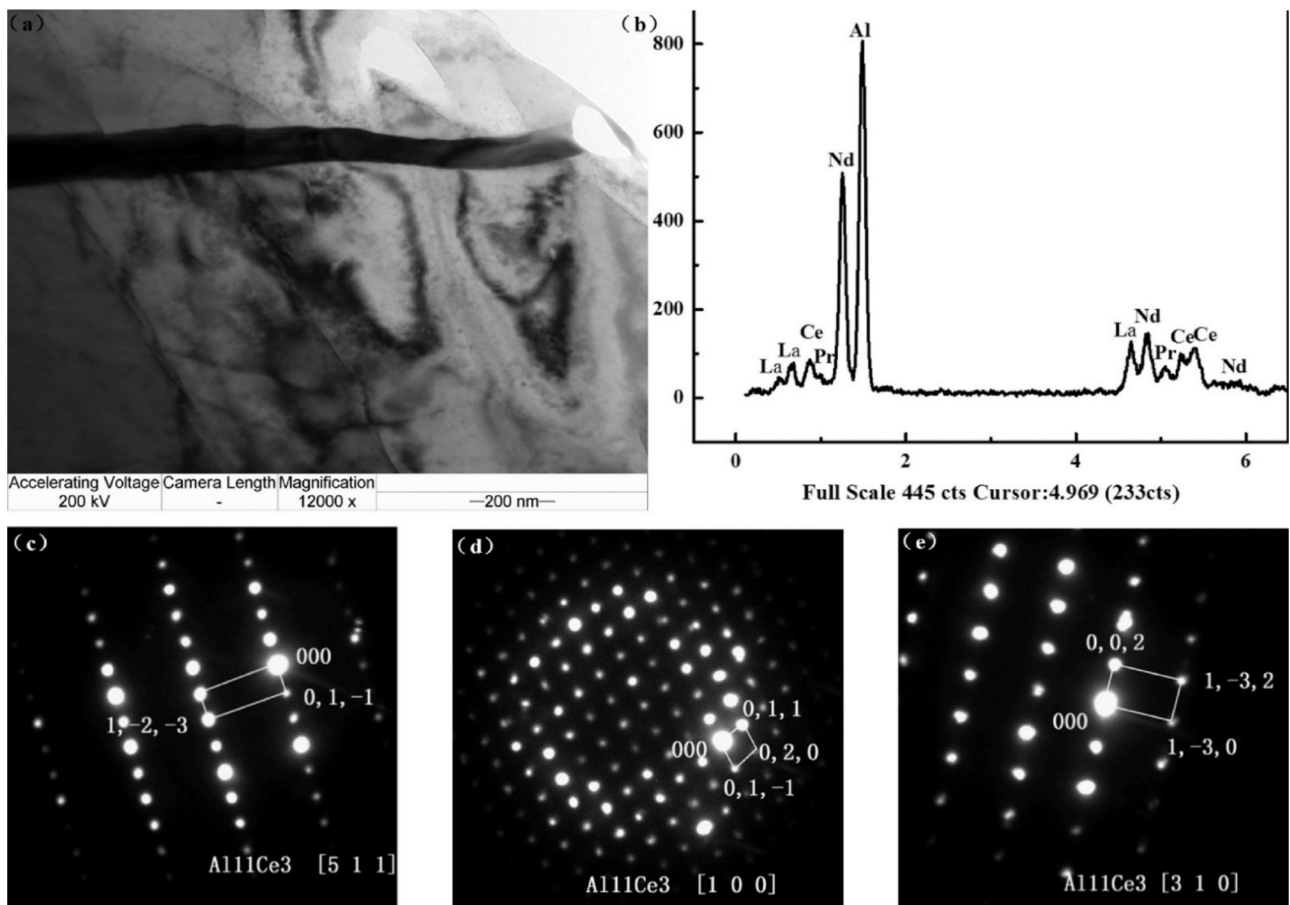


Figure 2. (a) TEM bright-field image; (b) EDX spectrum; and (c–e) SAED patterns ([511] zone, [100] zone, [310] zone axis, respectively) of the  $\text{Al}_{11}\text{Ce}_3$  precipitates in unreinforced AE44 alloy [95].

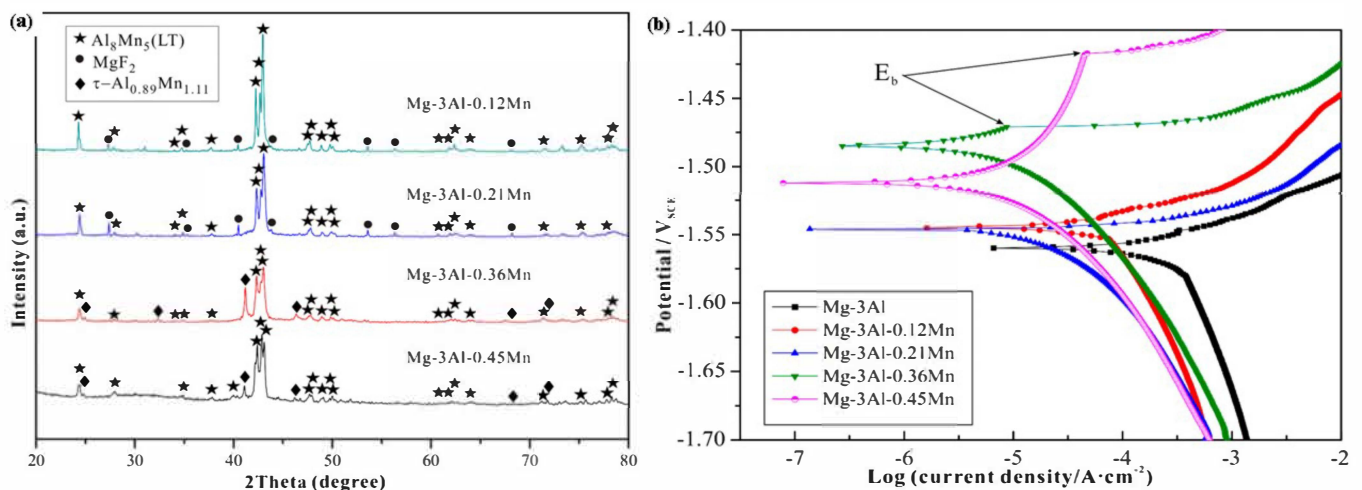
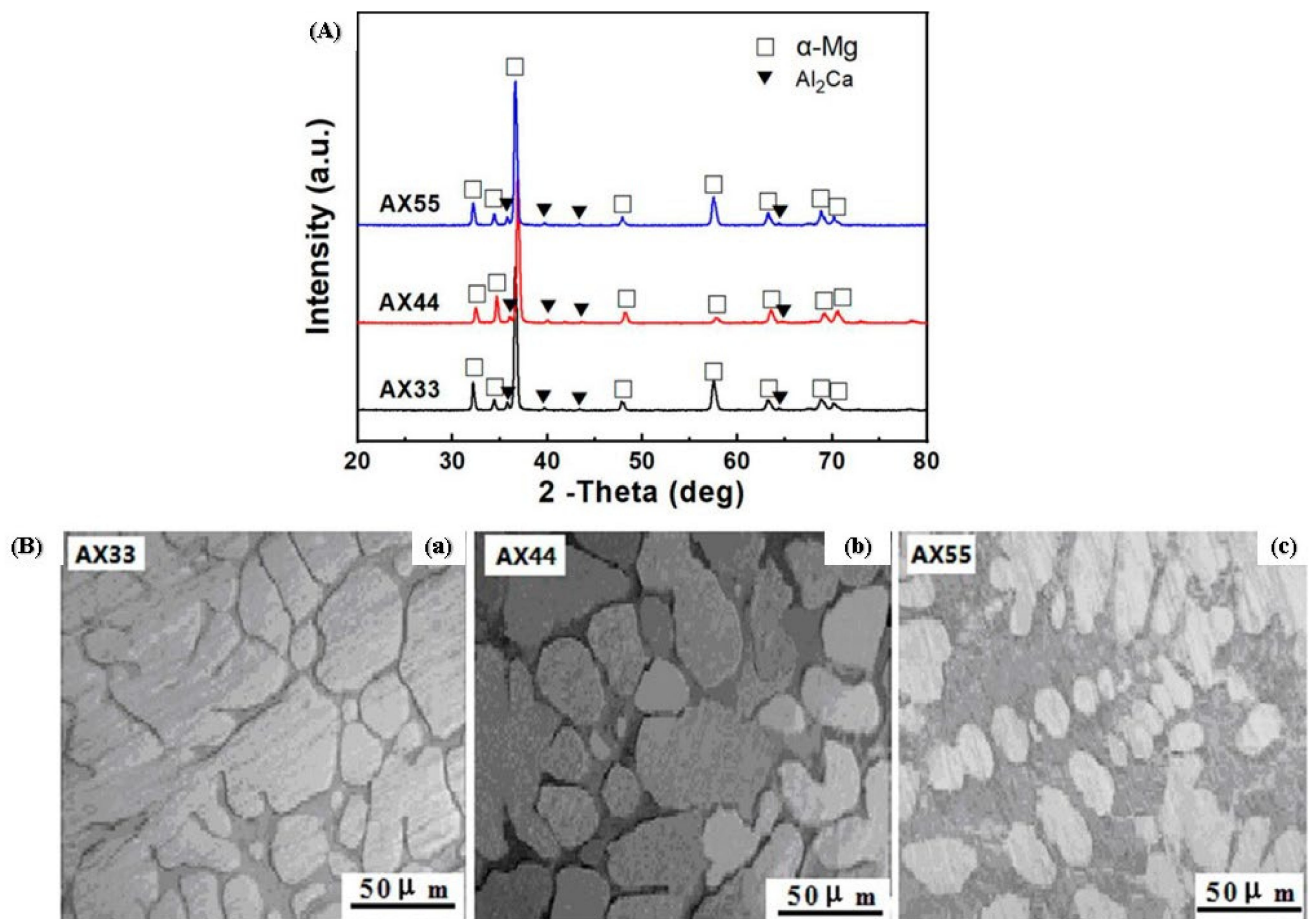


Figure 3. (a) XRD image of Mg-3Al-xMn alloys ( $x = 0.12, 0.21, 0.36, 0.45$ ). (b) Polarization curves of the Mg-3Al-xMn alloys ( $x = 0.12, 0.21, 0.36, 0.45$ ) in 3.5 wt.% NaCl solution, with the arrow indicating the breakdown potential ( $E_b$ ) [96].

The addition of alloying element, calcium enhances the strength of Mg-Al-based alloys due to the presence of a stable  $\text{Al}_2\text{Ca}$  phase in Mg-Al alloy [12]. For around 1.7 wt.% of calcium in Mg-2.32Al alloy, the refinement in grain occurs around the boundary which leads to an increase in UTS (ultimate tensile strength), elongation (%), and YS (yield strength) to

about 324 MPa, 10.2%, and 275 MPa respectively [50]. The FE-SEM imaging shows that the broken  $\text{Al}_2\text{Ca}$  phase is present which leads to improvements in the mechanical properties of the alloy. The comparative study of AZ31 alloy both with and without calcium shows that calcium in AZ31 provides better mechanical properties with finer grains and high ductility [11]. Kwak et al. concluded that calcium in AZ31 leads to a refinement in grain size and obtained a uniform composition of the alloy at 0.5 wt.% of calcium [91]. The alloys Mg-3.2Al-3.3Ca-0.7Mn (AX33), Mg-4.2Al-4.3Ca-0.7Mn (AX44), and Mg-5.1Al-5.2Ca-0.7Mn (AX55) were created to highlight the relationship between microstructure and characteristics of Mg alloys with high Ca/Al ratios. XRD images of all three alloys depicted the  $\alpha$ -Mg solid solution and  $\text{Al}_2\text{Ca}$  phase depicted in Figure 4A. It was further concluded that when the ratio of Ca/Al was less than 0.8, then the  $\text{Al}_2\text{Ca}$  phase formed but (Mg, Al) $_2$ Ca or (Mg, Al) $_2$ Ca +  $\text{Mg}_2\text{Ca}$  phases were produced when the Ca/Al ratio was more than 0.8 [97]. Figure 4B depicted the OM image of the as-cast ingots of AX33, AX44, and AX55, indicating that the as-cast ingots had the presence of reticular (Mg, Al) $_2$ Ca +  $\alpha$ -Mg solid solution. The grain boundary of the  $\alpha$ -Mg solid solution was dispersed with the reticular (Mg, Al) $_2$ Ca phase. As the amount of Ca and Al in the as-cast ingots increased, so did the volume percentage of the (Mg, Al) $_2$ Ca phase [97].



**Figure 4.** (A) XRD image of the as-extruded AX33, AX44, and AX55 alloys. (B) Optical microscopy of the as-cast ingots of (a) AX33, (b) AX44, and (c) AX55 alloy [97].

The alloying element strontium in Mg-Al-based alloy enhances the mechanical properties of the alloy due to the presence of a stable  $\text{Al}_4\text{Sr}$  compound [50]. The addition of 0.02 wt.% of strontium to double-hot-extruded Z80 alloy enhances the elongation (%) and UTS (ultimate tensile strength) to 13.2% and 355 MPa, respectively [62]. However, one research study suggested strontium decreases the solubility of aluminum in Mg alloys, as it hinders the formation of the  $\beta$ - $\text{Mg}_{17}\text{Al}_{12}$  phase, which has an adverse effect on mechanical

properties [93]. The increase in the amount of tin in AZ91 restricted the formation of the discontinuous  $\beta$ -Mg<sub>17</sub>Al<sub>12</sub> phase, but up to 4 to 5 wt.% of tin promotes reduction in the discontinuous  $\beta$ -Mg<sub>17</sub>Al<sub>12</sub> phase and improved the mechanical property as compared to AZ91 alloys, as the density of fine precipitates is continuously increasing [50]. The electromagnetic stirring of AZ91 alloy refines the  $\alpha$ -Mg and  $\beta$ -Mg<sub>17</sub>Al<sub>12</sub> grains (due to the rise in nucleation rate), and creates a few tensile twins, increasing the ultimate tensile strength, yield strength, and elongation to 187mpa, 167mpa, and 7.5%, respectively. Electromagnetic stirring increases the ductility of the AZ91 alloy, which has low plasticity and enhances the application field of AZ91 alloy [98]. XRD imaging of AZ91 alloy depicted the  $\alpha$ -Mg and  $\beta$ -Mg<sub>17</sub>Al<sub>12</sub> phase, but after electromagnetic stirring, there is only the  $\alpha$ -Mg matrix peak visible, reducing the volume of  $\beta$ -Mg<sub>17</sub>Al<sub>12</sub>. Figure 5A depicted the SEM image of AZ91 alloys, indicating the Mg matrix and white secondary phases ( $\beta$ -Mg<sub>17</sub>Al<sub>12</sub>). The unmodified sample involves the  $\alpha$ -Mg matrix,  $\beta$ -Mg<sub>17</sub>Al<sub>12</sub> phase and eutectic  $\alpha + \beta$  phases. The eutectic  $\alpha + \beta$  phase (lamellar) and  $\beta$ -Mg<sub>17</sub>Al<sub>12</sub> phase (coarse dendrites) are mainly distributed on the grain boundary. The modified sample of AZ91 alloy indicates the partial breaking of the eutectic  $\alpha + \beta$  phase and the reduction of the  $\beta$ -Mg<sub>17</sub>Al<sub>12</sub> phase resembling the more uniform dispersion of  $\beta$ -Mg<sub>17</sub>Al<sub>12</sub> phase induced by electromagnetic stirring [98]. EBSD mapping of AZ91 alloy shown in Figure 5B indicated low-angle grain boundaries (LAGBs) with misorientation within 2°–10°, which are designated by a white line, while high-angle grain boundaries (HAGBs) with misorientation larger than 10° are indicated by a black line. The microstructure of the unmodified specimen showed that the fraction of grains with a significant misorientation angle of 15°–90° is more uniform and that the proportion of grains with a misorientation angle less than 5° is relatively high [98]. The grains of the modified specimen contain a significant number of grains with LAGBs and fractured substructures together with a small number of {1012} tensile twins. Because of the occurrence of twinning inside the AZ91 alloy during the electromagnetic stirring, the HAGBs are primarily dispersed between 80° and 90°, and the misorientation angle distribution of 85°–90° existed in the sample. The TEM image of the AZ91 alloy is shown in Figure 5C indicating that the unmodified AZ91 alloy depicted some spherical particles (Mg<sub>17</sub>Al<sub>12</sub> phase) and a modified sample refined and uniformly distributed the Mg<sub>17</sub>Al<sub>12</sub> phase in the AZ91 alloy [98].

### 3.1.2. AM Alloy Series

The lanthanum and cerium enhance the ultimate strength and yield tensile strengths along with elongation in AM alloy series [96]. In AM50-1La alloy, the refinement in grain size provides more significant strength to lanthanum than cerium [97]. However, the addition of lanthanum and cerium together in AM50 alloy causes the reduction in mechanical properties of AM50 alloy due to the formation of coarse grain that reduced Mg<sub>17</sub>Al<sub>12</sub> phase precipitation [97]. The AM series have AM50 and AM60 alloy that have appropriate mechanical properties such as ductility, high strength, and high corrosion resistance [96]. The scarcity of REE (rare earth elements) allows calcium and tin to be used as alternative alloying elements in magnesium AM alloy [98]. The addition of calcium and tin in AM series alloy provides the refinement in grain size [2]. In hot-rolled AM30-0.5Zn, metal matrix alloy has a significant reduction in the size of grains in the matrix between the range from 240 $\mu$ m to 7 $\mu$ m [50]. The addition of cerium in AM50 alloy allows the formation of a rough Al<sub>11</sub>RE<sub>3</sub> phase and Al<sub>10</sub>Ce<sub>2</sub>Mn<sub>7</sub> phase [96]. The hot rolling process has significantly improved the ultimate tensile strength and yield strength to around 300 MPa and 230 MPa, respectively [99]. At 2 wt.% of neodymium in AM50 alloy was hot rolled to improve thermal stability and mechanical properties with no rough grains evolved [61]. The AM30-1Sn-xLi alloys have significantly improved the elongation (%) from 16% to 35% with a reduction in ultimate tensile strength when x varies from 5 wt.% to 11 wt.% due to change in crystal structure to BCC (body-centered cubic) as depicted in Figure 6 [50].

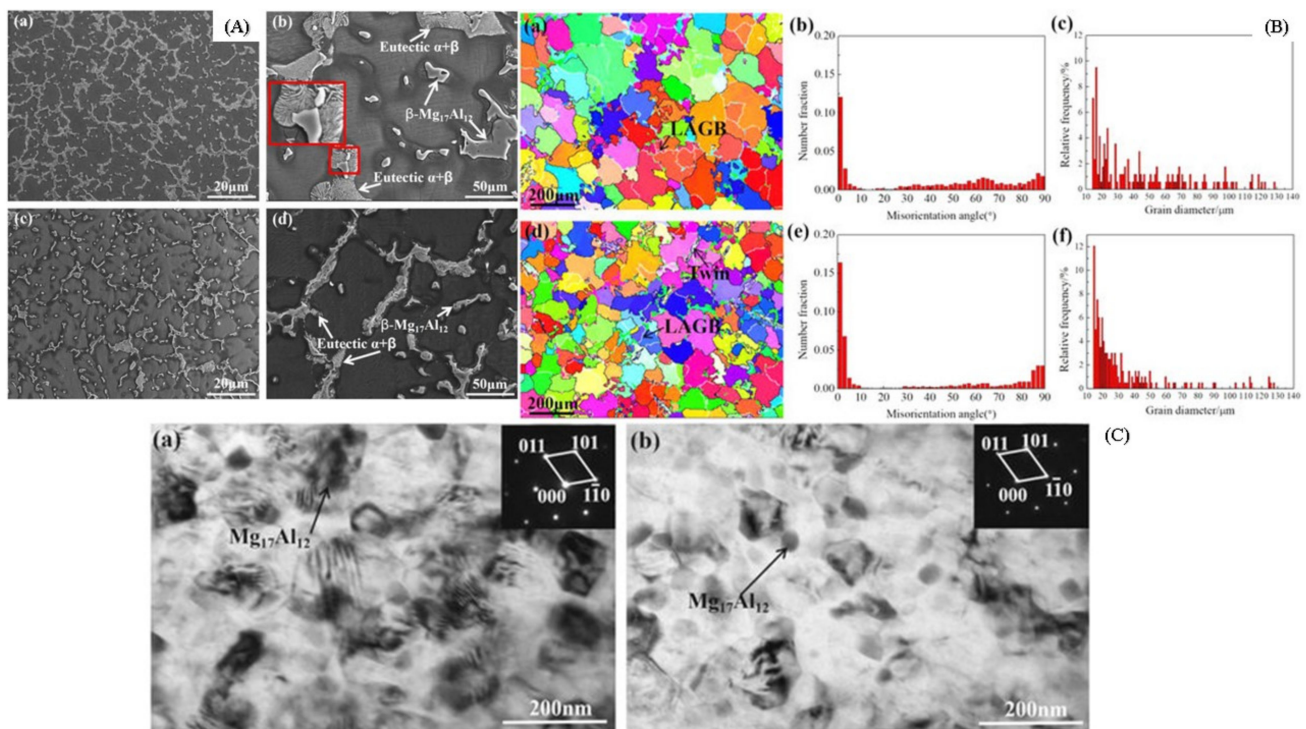


**Figure 5.** (A) SEM image of AZ91 alloy (a,b) unmodified sample, (c,d) modified sample. (B) For unmodified AZ91 alloy (a) EBSD mapping (b) Misorientation angle, and (c) Grain diameter distribution; For modified AZ91 alloy (d) EBSD mapping, (e) Misorientation angle, and (f) Grain diameter distribution. (C) Bright-field TEM image of AZ91 alloy (a) Unmodified, and (b) Modified sample [98].

The microstructure of AM50 alloy with and without the addition of Ce is depicted in Figure 6a–c [100]. It is clear that the  $\alpha\text{-Mg}$  and  $\beta\text{-Mg}_{17}\text{Al}_{12}$  phases make up the majority of the AM50 alloy's microstructure, particularly near grain boundaries. Porosity is another issue that frequently arises in high-pressure die casting and is primarily visible around the grain boundaries.  $\text{Al}_{11}\text{Ce}_3$  intermetallic phase is created when the additional Ce interacts with Al during solidification. This intermetallic phase solidifies before the  $\beta$ -phase, which reduces the amount of Al that is available for  $\beta$ -phase production.  $\text{Al}_{11}\text{Ce}_3$  actually forms even before the  $\alpha\text{-Mg}$  begins to solidify, serving as the a-nucleus phase and potentially refining the grain [100]. A notable reduction in grain size was not noticed, though. Figure 6d–f displays SEM images of the three alloys under investigation and an analysis of the phases using EDX in Figure 6g [100]. Ce addition decreases the amount of  $\beta$ -phase and encourages the creation of the  $\text{Al}_{11}\text{Ce}_3$  phase. The creation of the  $\text{Al}_{11}\text{Ce}_3$  phase and the reduction of the  $\beta$ -phase are both responsible for the improvement in corrosion resistance of AM50 alloy that occurs with increasing Ce content.

### 3.2. Mg-Zn Based Alloys

Zinc is considered one of the most commonly used alloying elements other than aluminum, which improves the mechanical properties of magnesium-based material alloys [75]. Compared with aluminum, zinc is regarded as a biocompatible alloying element alongside being seen as an important element present in the body, fulfilling nutrient availability. Therefore, it is regarded as the most suitable alloying element used in biomedical applications [78]. The main components/phases depicted in Mg-Zn alloy are  $\alpha\text{-Mg}$  and  $\text{Y-MgZn}$  phases [100]. The solubility of zinc in magnesium is found to be highest at around 6.2 wt.% but drops sharply to about 2.6 wt.% [50]. The increase in the concentration of zinc content increases the YS (yield strength) of the Mg-Zn alloy and the ultimate tensile strength (216.8 MPa) and elongation (15.8%) and obtained to be maximum of around 4 wt.% of zinc [101]. Adding alloying elements such as zirconium, calcium, silicon, yttrium,

strontium, and manganese provides a significant improvement in the mechanical properties of magnesium–zinc-based alloys [8]. Figure 7a indicates the optical energy band gap ( $E_g$ ) of  $Mg_xZn_{1-x}O$  thin films (function of  $Mg^{2+}$  concentration), and Figure 7b showed the tabulated data representing the optical band gap, RMS, and grain size for AFM image of  $Mg_xZn_{1-x}O$  thin film [102]. The successive ionic layer adsorption and reaction (SILAR) approach was used to generate a sequence of  $Mg_xZn_{1-x}O$  thin films on glass substrates. It has been noted that the deposited films are polycrystalline in nature and have grown in hexagonal and cubic phases [102]. The film preferred orientation was absorbed along the {002} plane. As the  $Mg^{2+}$  ions content rises, the crystallite size and surface roughness also do. The outcomes thus demonstrated that the  $Mg^{2+}$  ions content can regulate the surface topography and surface quality of the deposited films [102]. The optical transmittance spectra investigation revealed that the energy band gap increased (2.82–3.17 eV) as the  $Mg^{2+}$  concentration increased for  $x = (0.25–0.75)$ , and the transmittance increased with the rise of  $Mg^{2+}$  content to around 85% [102]. These findings suggest that high-performance ultraviolet optoelectronic devices may be made using  $Mg_xZn_{1-x}O$  thin films. The various alloying elements employed in the Mg–Zn alloys are listed below.

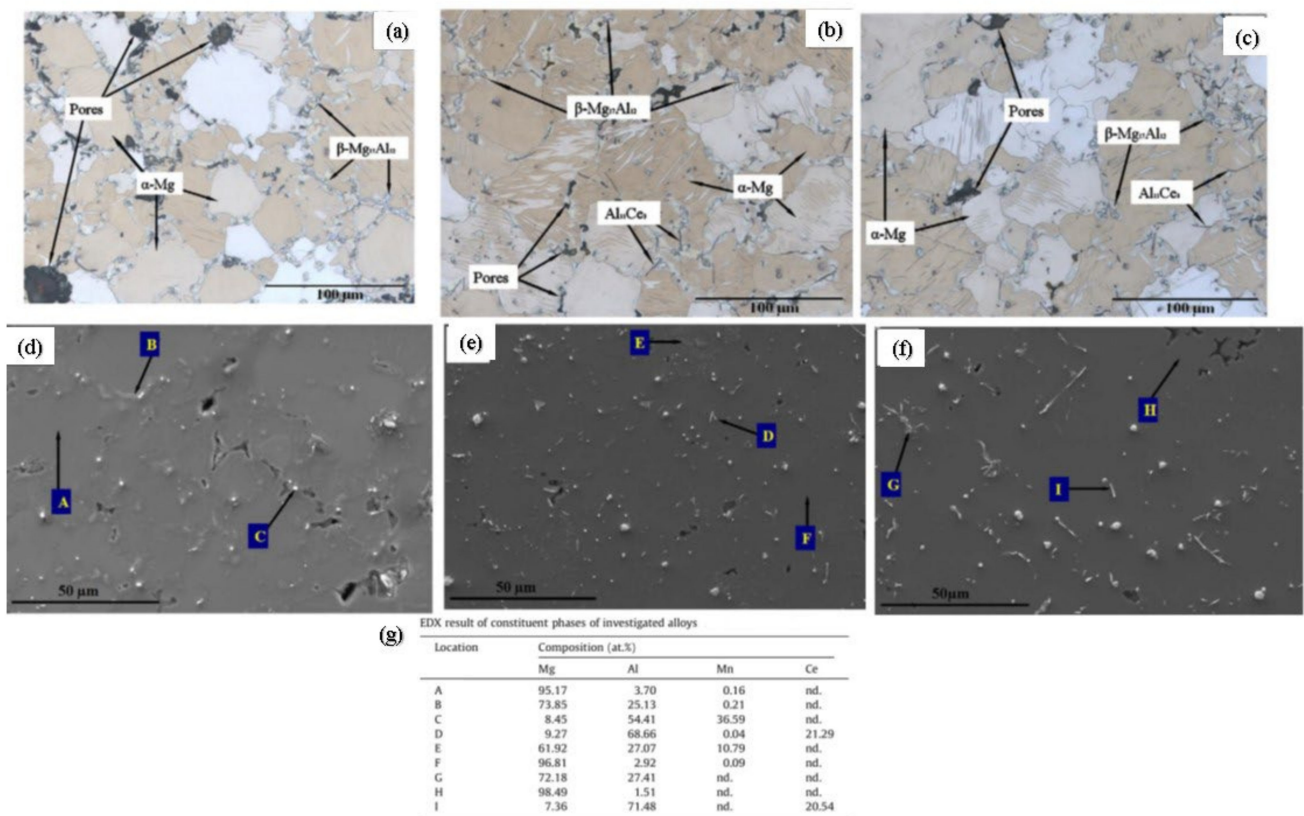


**Figure 6.** Optical Microstructure of alloy (a) AM50 (b) AM50Ce0.5 (c) AM50Ce1; SEM imaging of alloy highlighting the Location of points described in EDX for (d) AM50 (e) AM50Ce0.5 (f) AM50Ce1; (g) EDX result of AM50, AM50Ce0.5, and AM50Ce1 describing the location of points of SEM in (d–f) (nd indicated not displayed) [100].

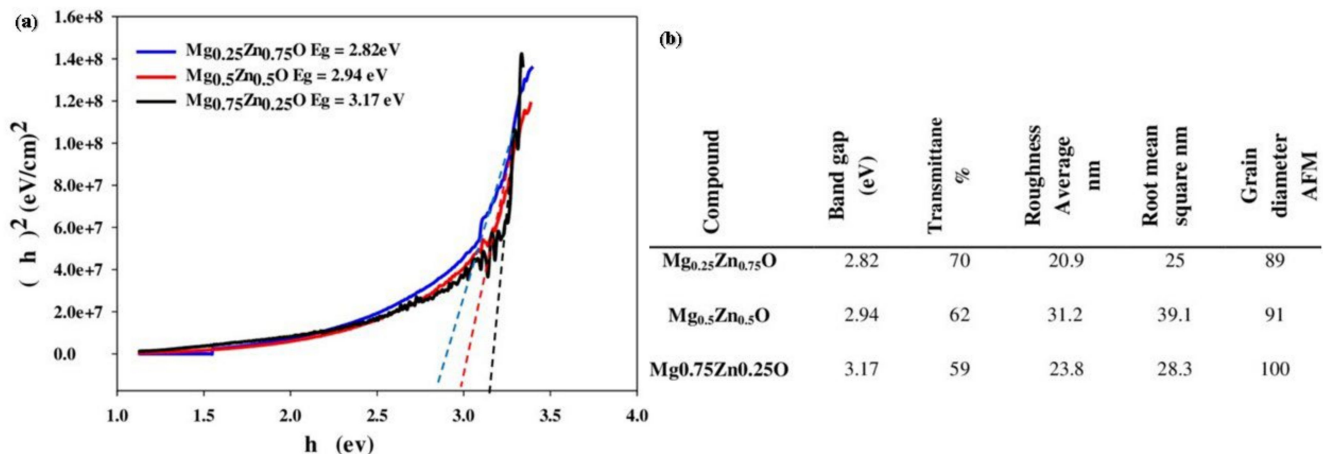


**Figure 7.** (a) Optical energy band gap ( $E_g$ ) of  $Mg_xZn_{1-x}O$  thin films (function of  $Mg^{2+}$  concentration), (b) Tabulated data representing the optical band gap, RMS, and grain size for AFM image of  $Mg_xZn_{1-x}O$  thin film [102].

### 3.2.1. Mg-Zn-Ca Alloys

Mg-Zn-Ca alloy is cost-effective and has superior mechanical properties among all Mg-Zn alloys [11]. The presence of calcium in Mg-based alloy acts as a grain refiner [11]. However, the mechanical properties of Mg-Zn-based alloys are reduced when the concentration of calcium increases beyond 1% due to the reduction in the solubility of calcium [10]. The research study suggested that the Mg-1Zn-0.5Ca alloy results in an improvement in mechanical properties of the alloy at hot extrusion due to the refinement in grain size and weakening of base texture via 0.5 wt.% Ca in Mg-Zn alloy [103]. The ultimate tensile strength was observed to be maximum up to 1 wt.% of Ca in Mg-Zn alloy due to the formation of sharp substrate texture, and partial recrystallization of microstructure [103]. The surface morphology of the alloy Mg-4.0-Zn-0.2-Ca indicated by optical microscopy is illustrated in Figure 8a,b of the Mg-4.0-Zn-0.2-Ca alloy [104]. The researchers experimentally verified that the extruded Mg-Ca-Zn-Zr alloy was tested with a low concentration of Zn and Ca content, i.e., around 1 wt.%, obtained the elongation (11%) and tensile strength (306 MPa) [50]. The Zener pinning dynamic recrystallization of fine precipitates refines the microstructure of magnesium–calcium-based alloys [74]. The research study analyzed the addition of 0.8 wt.% Zr in Mg-6Zn-0.2Ca alloy (ZX60) showed an improvement in tensile yield strength from 148 MPa to 310 MPa [104]. When manganese, calcium, and zinc are added in a dilute state, it exhibits balanced ductility and yield strength along with an improvement in the extrudability of the alloy subtending to high specific strength that widens the application of Mg-based alloy, making it suitable for broad industrial applications [50].

### 3.2.2. Mg-Zn-Mn Alloys

Mg-Zn-Mn alloy has high strength, excellent resistance to corrosion, and high ductility [50]. The extruded Mg-5.99Zn-1.76Ca-0.35Mn alloy has superior mechanical properties involving a yield strength of 289MPa and an elongation of 16% [91]. With the addition of 0.3% of Mn in Mg-Zn-Ca alloy, the improvement in yield strength was observed and obtained to be 50MPa, but the addition of about 2 wt.% of Mn to extruded Mg-2Zn alloys, also improved the yield strength and ductility of alloy along with the refinement in grain size and produced the improvement in sliding resistance [105]. The research study suggested that the addition of manganese improves the tensile strength and ductility of pure Mg by around 204.3 MPa and 38.8% respectively [27]. Along with manganese, the addition of silicon to Mg-Zn alloy improves the yield tensile strength of the alloy and is observed to be around 200–240 MPa [105–108]. A significant density of Al, Mn intermetallic particles can be seen in the matrix in Figure 9a,b representing FE-SEM/EDS imaging and AFM

imaging of  $\beta$ -Mg<sub>17</sub>(Al, Zn)<sub>12</sub> precipitates,  $\alpha$ -Mg solid solution, and Al, Mn particles after mechanical polishing [99]. FE-SEM/EDS measurements revealed a composition of  $38.1 \pm 2.1$  (%) Al and  $44 \pm 5$  (%) Mn. These particles have a diameter of 0.5 to 5  $\mu$ m. The results of the FE-SEM/EDS studies showed that they were composed of Mg (61.3%), Al (64.4%), Zn (3.4%), O (1%), Mn (0.3%), Ni (0.37%), and Cu (0.2%). AFM imaging did not identify any micro-voids at the point where the massive precipitates contacted the metallic matrix [99].

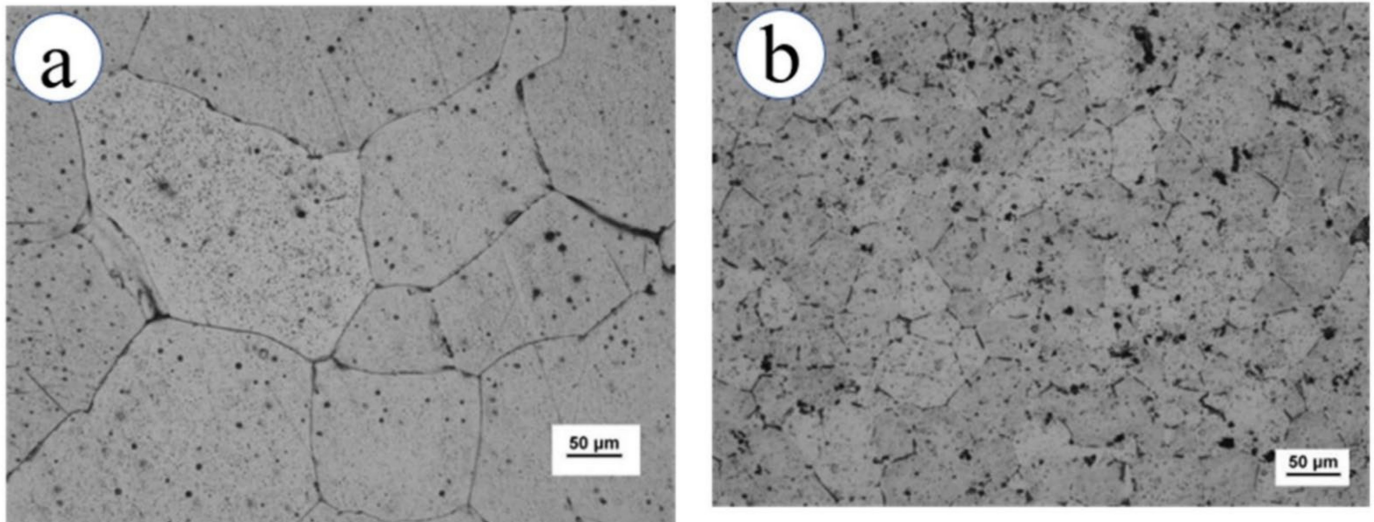


**Figure 8.** (a,b) Optical micrograph of Mg-4.0-Zn-0.2-Ca [104].

### 3.2.3. Mg-Zn-RE-Based Alloys

To improve the ductility and strength of the Mg-Zn extruded alloys, rare earth elements are added to the Mg-Zn alloy [106]. When weak RE components are added, the fundamental structure of Mg-Zn alloys becomes fragile. The alloy gains strength as strengthening particles develop as RE and zinc concentration levels are raised, but its ductility rapidly decreases. Research on the extruded Mg-Zn-Ce alloys has been particularly focused on their ductility. The ductility of extruded Mg-2Zn-0.2Ce alloy was found to be around 27% [107]. The ductility of Mg-2Zn-0.2Ce was demonstrated to be around 10% higher than AZ31 alloy under identical extrusion conditions. The ductility of Mg-Zn-Ce decreased to 50% with the addition of more than 5 wt.% of Zn, while the yield strength remained unaffected [108,109]. Zirconium is therefore added to such alloys with more than 5 wt.% of Zn in order to increase ductility and strength. With a high proportion of Zn (5 to 6 wt.%), Mg-Zn-Ce-Zr alloys have yield strengths of about 247–330 MPa and elongations between 17 and 27% [107–110]. Extruded Mg-Zn-Ce-Zr alloys and ZK60 alloys, each having 0.5 wt.% of Zr and 6wt.% of Zn, were compared, and it was found that the alloy with additional Ce had higher tensile strength and increased the density and adjusted precipitate size during extrusion [111]. The technique of Selected Area Electron Diffraction (SAED) is crucial for figuring out the crystal structure of any substance. Figure 10 depicted the TEM micrographs of (a1) Mg-6Zn-0.5Zr-0.5Ce, (a2) Mg-6Zn-0.5Zr-1Ce, and (a3) Mg-6Zn-0.5Zr-1.5Ce alloy, SAED pattern of (b1) Mg-6Zn-0.5Zr-0.5Ce (b2) Mg-6Zn-0.5Zr-1Ce, and (b3) Mg-6Zn-0.5Zr-1.5Ce alloy [111]. ZK60 was made more extrudable by cerium (Ce). However, multiple cracks can be seen in ZK60, although the Mg-6Zn-1Zr-1Ce alloy exhibits fewer defects under the same extrusion circumstances [112].

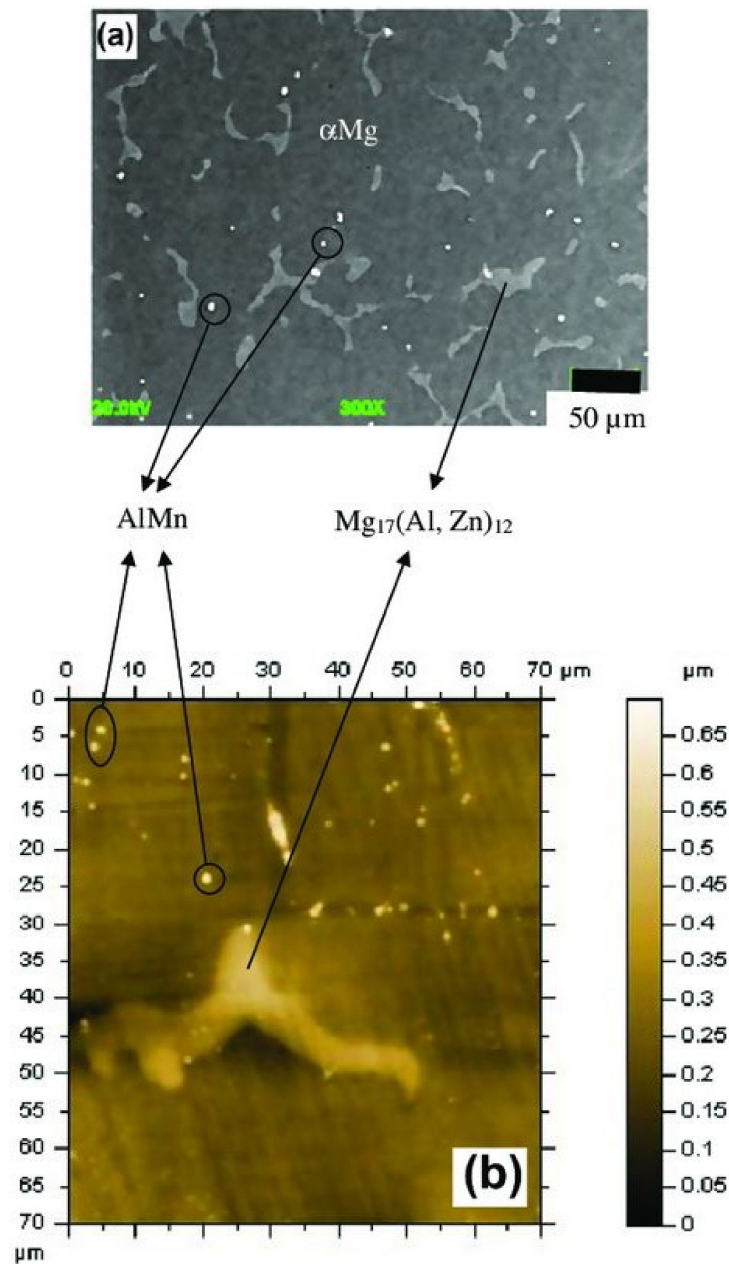


**Figure 9.** (a) FE-SEM/EDS imaging (b) AFM imaging of  $\beta\text{-Mg}_{17}(\text{Al}, \text{Zn})_{12}$  precipitates,  $\alpha\text{-Mg}$  solid solution, and Al, Mn particles after mechanical polishing [99].

Compared to calcium (Ca) alone, rare earth elements and Ca combined have significantly improved the strength of alloys. In comparison to extruded Mg-Zn-Ce or Mg-Zn-Ca alloys, the results of extruding Mg-5.3Zn-0.2Ca-0.5Ce and Mg-2.5Zn-0.2Ca-0.4La alloys showed greater yield tensile strengths (268 MPa and 325 MPa, respectively) [112]. Mg-Zn and Mg-Zn-Ca alloys have denser precipitate distributions, according to the microstructural analysis of these alloys. When cerium (Ce) or lanthanum (La) is added to Mg-Zn-Ca alloy as precipitation density, a robust alloy is created in hot extrusion improved [113,114]. Liu et al. [115] investigated the microstructure and mechanical properties of Mg-5Zn-0.3Y-0.2Ce-xCa ( $x = 0, 0.3, 0.6$  wt.%) alloys. Figure 11 illustrates the OM and SEM image of the Mg-5Zn-0.3Y-0.2Ce-xCa ( $x = 0, 0.3, 0.6$  wt.%) alloys suggested that the addition of Ca (0.3, and 0.6 wt.%) formed more lamellar eutectic microstructure. Figure 11a,d. The detached second particles are spread across grain boundaries and inter-dendritic regions, as shown in Figure 11a,d, while the addition of Ca (0.3, and 0.6 wt.%) formed the more

lamellar eutectic microstructure. The grain size of the primary Mg phase was observed to be reduced for 0.6 wt.% of Ca and obtained to be 300  $\mu\text{m}$ , 180  $\mu\text{m}$ , and 145  $\mu\text{m}$  for  $x = 0, 0.3,$  and  $0.6$  wt.% in Mg-5Zn-0.3Y-0.2Ce- $x$ Ca alloy indicated in Figure 11a–c. In as-cast Mg-5Zn-0.3Y-0.2Ce-0.6Ca alloy, the lamellar second phases increased noticeably and created a continuous network. The second phases are identified as  $\text{MgYZn}_6$ , Mg-Zn-Ce, and  $\text{Ca}_2\text{Mg}_6\text{Zn}_3$  phases for  $x = 0, 0.3,$  and  $0.6$  wt.% in Mg-5Zn-0.3Y-0.2Ce- $x$ Ca alloy, respectively, depicted in Figure 11d–f. The high-angle annual dark field (HAADF) STEM imaging of Mg-5Zn-0.3Y-0.2Ce-0.6Ca alloy depicted in Figure 12 indicated that a lot of broken particles with an average size of 500 nm were scattered along the extrusion direction. The majority of the particles were enriched in Mg, Zn, and Ca, according to the EDS elemental mapping displayed in Figure 12b–f [115]. The precipitate was  $\text{Ca}_2\text{Mg}_6\text{Zn}_3$ , according to the SAED patterns. Due to the decreased mix entropy, Zn and Ca were simple to precipitate as Ca-Zn clusters during the extrusion. The extrusion process precipitated the nano-particles recommended in the work–study.

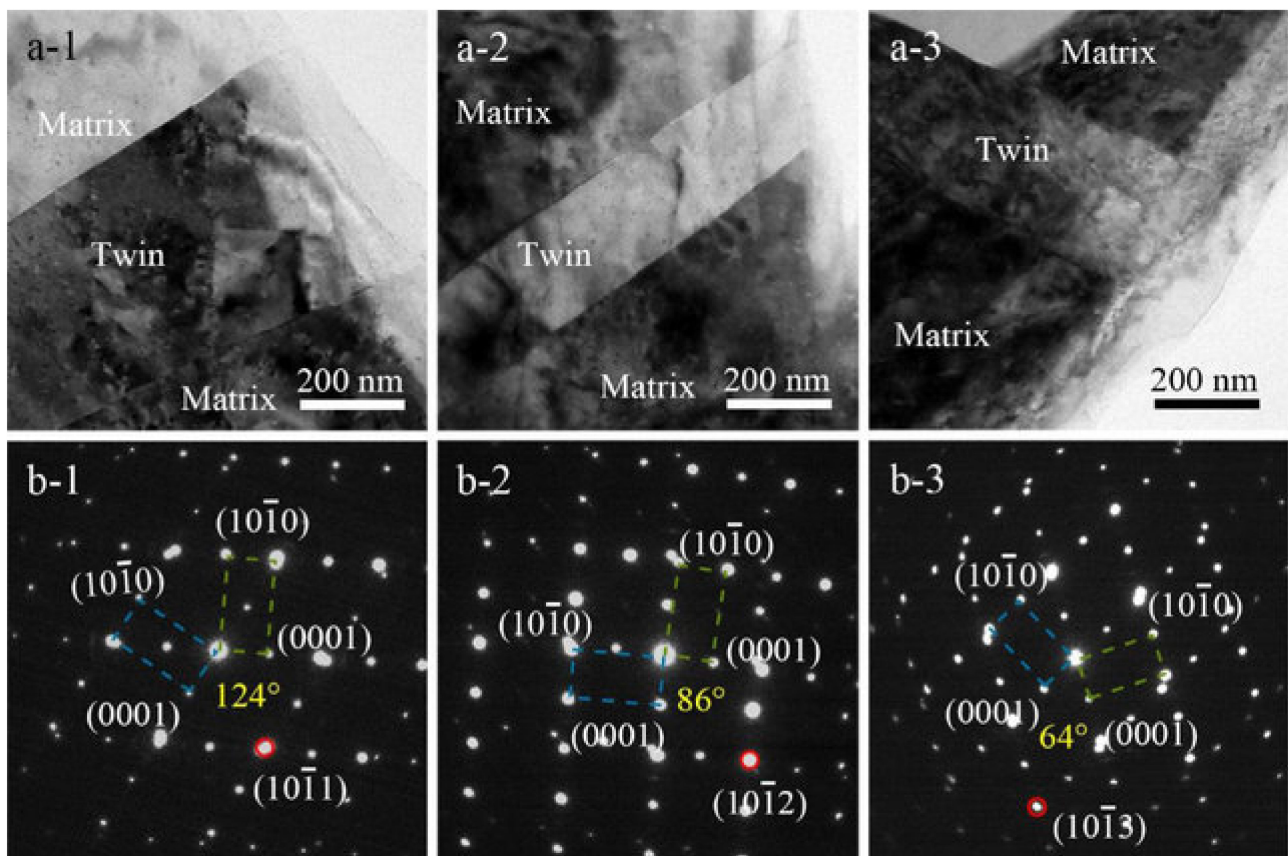


**Figure 10.** TEM micrographs of (a-1) Mg-6Zn-0.5Zr-0.5Ce, (a-2) Mg-6Zn-0.5Zr-1Ce, and (a-3) Mg-6Zn-0.5Zr-1.5Ce alloy, SEAD pattern of (b-1) Mg-6Zn-0.5Zr-0.5Ce (b-2) Mg-6Zn-0.5Zr-1Ce, and (b-3) Mg-6Zn-0.5Zr-1.5Ce alloy [111].

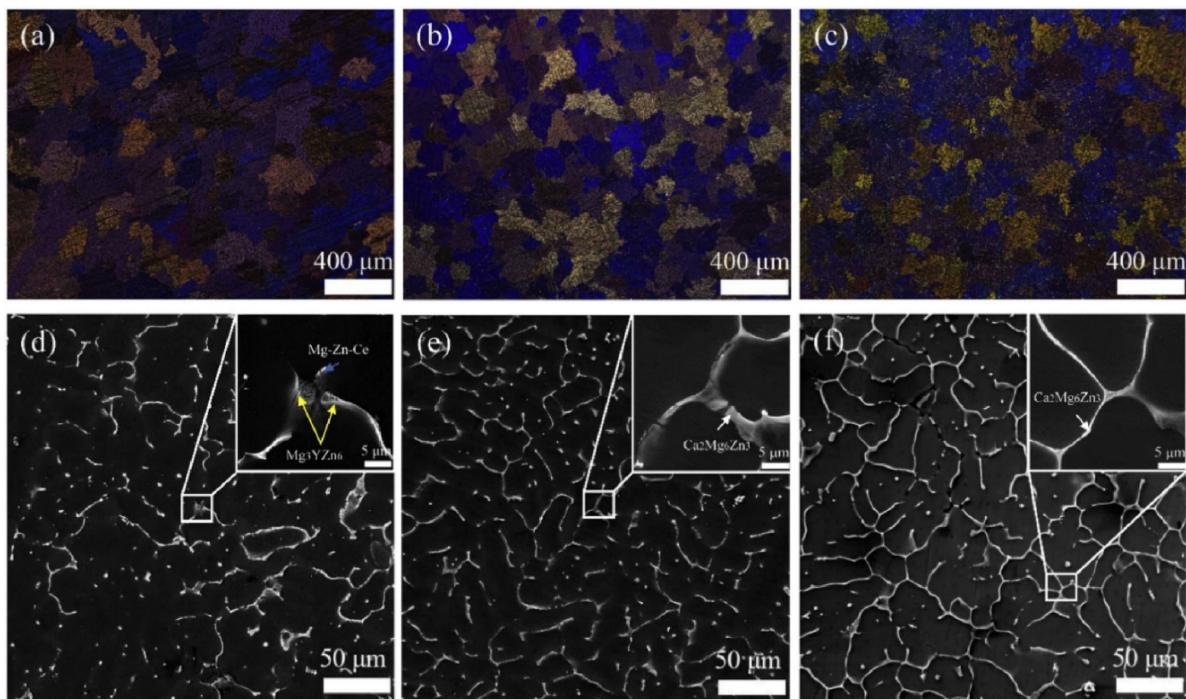


**Figure 11.** Optical Microscopy of Mg-5Zn-0.3Y-0.2Ce-xCa alloy (a)  $x = 0$  wt.%, (b) 0.3 wt.% and (c) 0.6 wt.%; and SEM micrographs of Mg-5Zn-0.3Y-0.2Ce-xCa alloy (d)  $x = 0$  wt.%, (e) 0.3 wt.%, (f) 0.6 wt.% [115].

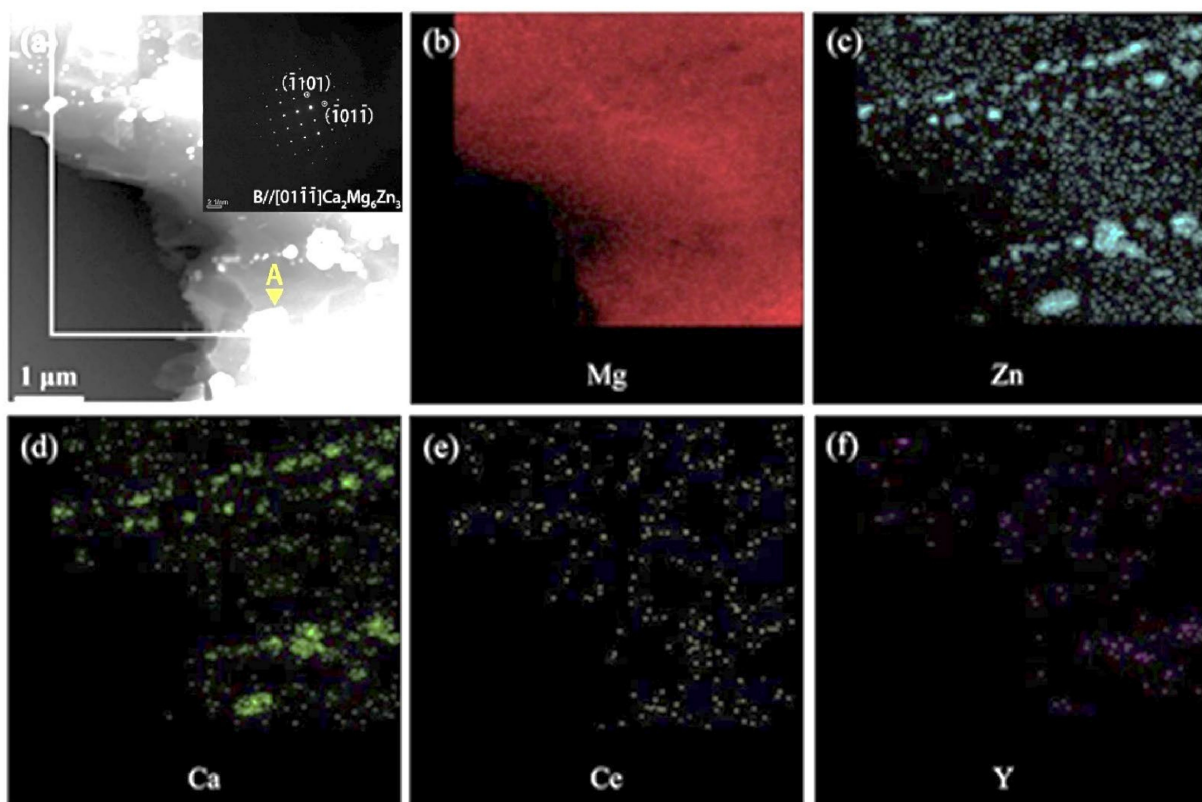


**Figure 12.** (a) Nanoparticles and precipitates in the as-extruded Mg-5Zn-0.3Y-0.2Ce-0.6Ca alloy: (a) HAADF-STEM image; (b–f) elemental mappings of Mg, Zn, Ca, Ce and Y [115].

The mechanical and extrusion properties of Mg-Zn alloys were enhanced by the addition of gadolinium. The yield strength of Mg-Zn-Gd alloy is typically between 200 and 300 MPa [114]. Given that gadolinium (Gd) is more soluble in magnesium than cerium, Mg-2Zn-1.5Gd alloy has a better yield strength (YS) of 50–60 MPa than Mg-2Zn-0.5Ce alloy under the same extrusion conditions as depicted in Figure 11 [112–114]. Lower Gd and Zn percentages increase the strength of Mg-Zn-Gd alloys [113]. Mg-5Zn-0.5Gd alloy has a higher yield strength (291 MPa) than Mg-6.8Zn-2.8Gd alloy (228 MPa) under similar extrusion conditions. According to other research studies, Mg-2Zn-Gd alloys have a higher yield potential than Mg-5Zn-Gd alloys because they contain a thermally stable second phase that does not melt during homogeneous processing of high concentration alloys [114]. A low rate of corrosion of less than 0.28 mm per year was observed in the Mg-1.8Zn-0.2Gd alloy [115]. L929, MG63, and VMSC cells had an in vitro cell viability of more than 80% and had no cytotoxicity [114–116]. For the first 2 months inside the body, the structure was undamaged. After 6 months, in-vivo studies showed very few residuals, demonstrating the excellent biodegradability of Mg-Zn-Gd alloys as implants. The alloy's mechanical properties (284 MPa YS, 338 MPa UTS, and 24% elongation) increased with further extrusion, and Hank's solution further improved the alloy's corrosion resistance. The improvement in mechanical characteristics is due to homogeneous microstructure with dispersed secondary phases and uniformly sized grains.

The research study on Mg-5.6Zn-0.55Zr-0.9Y alloy demonstrated that the addition of yttrium improved Mg-Zn alloy corrosion resistance (1.7% loss in mass after 242 h in Simulated body fluid) [117]. ZEK100 (1 wt.% of Zn, 0–5 wt.% of Zr, and 0–5 wt.% of RE), a material for biodegradable implants has good mechanical qualities that encourage bone development [118]. After the complete breakdown, ZEK100 research revealed its harmful consequences on tissue. Additionally, after implantation (in vivo), a weight reduction of about 7.5% and a reduction in pull-out forces of 44% were noted. This demonstrates that ZEK100, which is initially stable and degrades at a positive rate, is ideal for use in biodegradable implants [116–118]. Further, the addition of neodymium improved the mechanical characteristics and corrosion resistance of Mg-Zn- RE-based alloys [119].

### 3.3. Mg-Ca Alloy

Mg-Ca alloys have been studied for their degradation behavior and mechanical integrity, and results suggest that the addition of Ca lowers the degradation rate [120]. The alloying element calcium enhanced the corrosion behavior of Mg alloys [121]. In a modified simulated bodily fluid (SBF) immersion test, AZ91-Ca showed a decrease in its UTS of 15% and an elongation of its fracture of 20%. The research study analyzed the 1–20 wt.% of Ca in Mg alloy and examined its biodegradability in bone [122–124]. A high concentration of calcium in Mg-Ca alloys (5 wt.%, 10 wt.%, and 20 wt.% of Ca) displayed brittle behavior [125]. By reducing the concentration of Ca in Mg alloy, the mechanical characteristics and corrosion behavior of the Mg-Ca alloy were observed to be improved [125–131]. For as-cast Mg-Ca alloy samples, the UTS, YS, and elongation reduced as the Ca concentration increased [131]. The findings of the cytocompatibility evaluation showed that Mg-1Ca alloy does not cause cell toxicity [132]. The Mg-1Ca alloy surface formed a mixture of Mg(OH)<sub>2</sub> and HAp layer during the immersion and implantation periods, according to both in vitro and in vivo evaluations [132]. The work-study by Rad et al. suggested that due to its great corrosion resistance, the Mg-0.5Ca alloy is a good choice for biodegradable implants [132]. The compressive and tensile strength was enhanced with the addition of Ca, while the ductility decreased [133]. The researchers recommended that Ca and Zr are most suitable for grain refining and contribute to the alloy's improved mechanical performance for orthopedic applications [134–136].

The findings of the phase study recognized the intermetallic phases  $\alpha$ -Mg, Mg<sub>2</sub>Ca, Ca<sub>2</sub>Mg<sub>6</sub>Zn<sub>3</sub>, and Mg<sub>26</sub>Zn<sub>59</sub>Gd<sub>7</sub> in Mg<sub>5</sub>Ca-xZn1Gdx alloys (x = 1, 2, 3 wt.%) as shown in Figure 13A [137,138]. It was further observed that a reduction in Ca concentration in the alloy with the addition of Gd content formed a small volume of secondary phase

( $\text{Mg}_2\text{Ca}$  and  $\text{Ca}_2\text{Mg}_6\text{Zn}_3$ ). Additionally, the volume of the  $\text{Mg}_{26}\text{Zn}_{59}\text{Gd}_7$  phases had slightly increased with the addition of up to 2 wt.% of Gd. Beyond 2 wt.% of Gd, no visible changes were observed in the microstructure. The  $\text{Mg}_2\text{Ca}$ ,  $\text{Ca}_2\text{Mg}_6\text{Zn}_3$ , and  $\text{Mg}_{26}\text{Zn}_{59}\text{Gd}_7$  phases have a hexagonal microstructure. The lattice parameters for the Gd-containing compounds are illustrated as  $a = 14.633\text{\AA}$ ,  $b = 14.633\text{\AA}$ , and  $c = 8.761\text{\AA}$ . These lamellar phases (lengths around 100 nm) are distributed along the inter-dendritic regions as shown in Figure 13B [134]. The  $\text{MgCa}_5\text{-xZn}_1\text{Gd}_x$  alloys ( $x = 1, 2, 3$  wt.%) resemble to dendrite microstructure having inter-dendritic solute-rich area. The SEM image of  $\text{MgCa}_5\text{-xZn}_1\text{Gd}_x$  alloys ( $x = 1, 2, 3$  wt.%) depicted the primary  $\alpha\text{-Mg}$  phase and eutectic phase ( $\alpha\text{-Mg} + \text{Mg}_2\text{Ca}$ ), ( $\alpha\text{-Mg} + \text{Mg}_2\text{Ca} + \text{Ca}_2\text{Mg}_6\text{Zn}_3$ ), and ( $\alpha\text{-Mg} + \text{Mg}_{26}\text{Zn}_{59}\text{Gd}_7$ ) around the grain boundary as shown in Figure 13C. The reduction in the volume of the eutectic phase was observed with the amount of Gd due to the presence of the intermetallic phases ( $\text{Ca}_2\text{Mg}_6\text{Zn}_3$  and  $\text{Mg}_2\text{Ca}$ ) occupying the grain boundary. Furthermore, the Gd-containing phases that are distributed along the inter-dendritic area appeared as bright [138]. The SEM-corresponding EDS spectra ( $\text{MgCa}_3\text{Zn}_1\text{Gd}_2$  alloy) depicted the eutectic area (inter-dendritic region) indicated in Figure 14a–c. The region consisting of Mg with a higher concentration of Ca than Zn concentration resembles the  $\text{Mg}_2\text{Ca}$  phase depicted in Figure 14a. The region of Mg, Ca, Zn, and Gd resemble the  $\text{Mg}_{26}\text{Zn}_{59}\text{Gd}_7$  phase depicted in Figure 14b. Lastly, the region of Mg, Ca, and Zn resembles the  $\text{Ca}_2\text{Mg}_6\text{Zn}_3$  and  $\text{Mg}_2\text{Ca}$  phases depicted in Figure 14c [138].

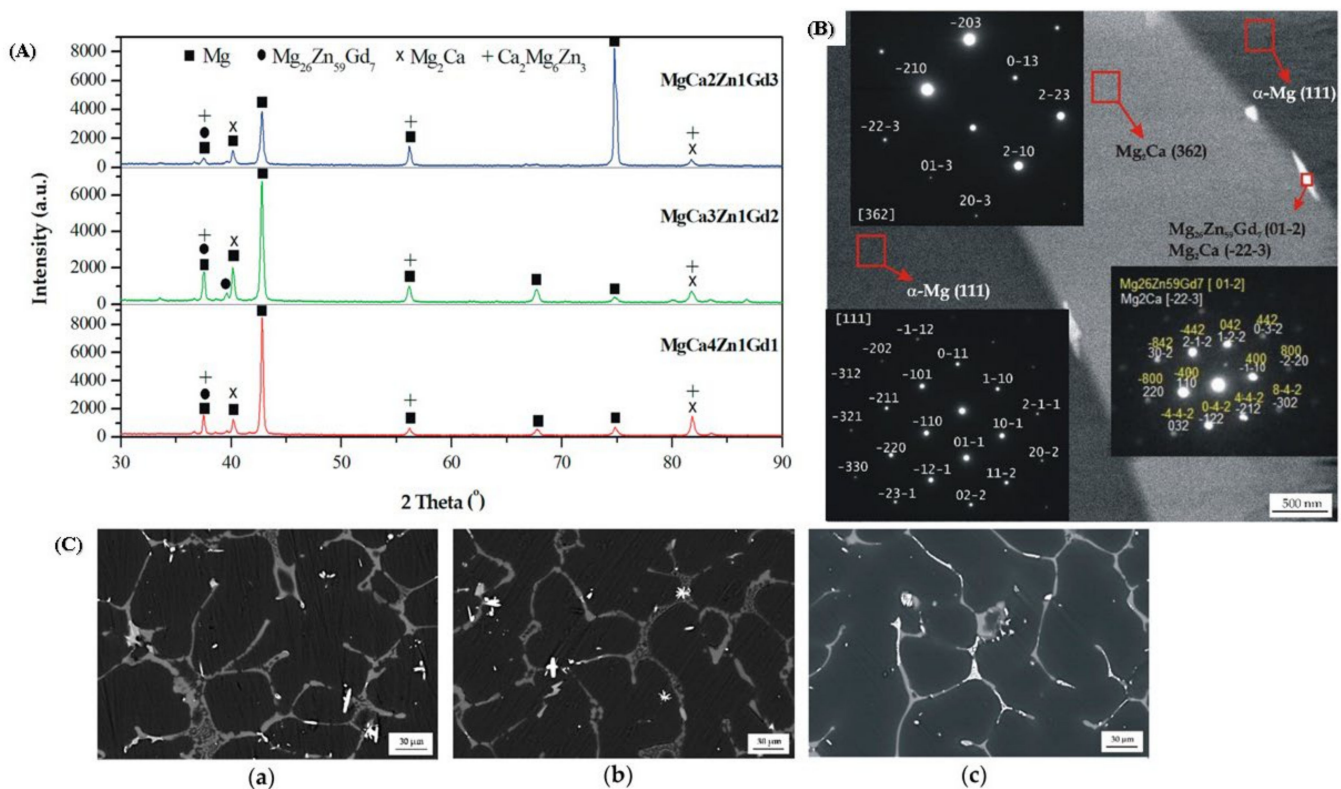


**Figure 13.** (A) XRD image of  $\text{MgCa}_{5-x}\text{Zn}_1\text{Gd}_x$  ( $x = 1, 2,$  and  $3$  wt.%) alloys (B) TEM micrograph and corresponding SAED patterns from selected areas of the  $\text{MgCa}_2\text{Zn}_1\text{Gd}_3$  alloy (C) SEM imaging of (a)  $\text{MgCa}_4\text{Zn}_1\text{Gd}_1$  (b)  $\text{MgCa}_3\text{Zn}_1\text{Gd}_2$  and (c)  $\text{MgCa}_2\text{Zn}_1\text{Gd}_3$  alloys [138].

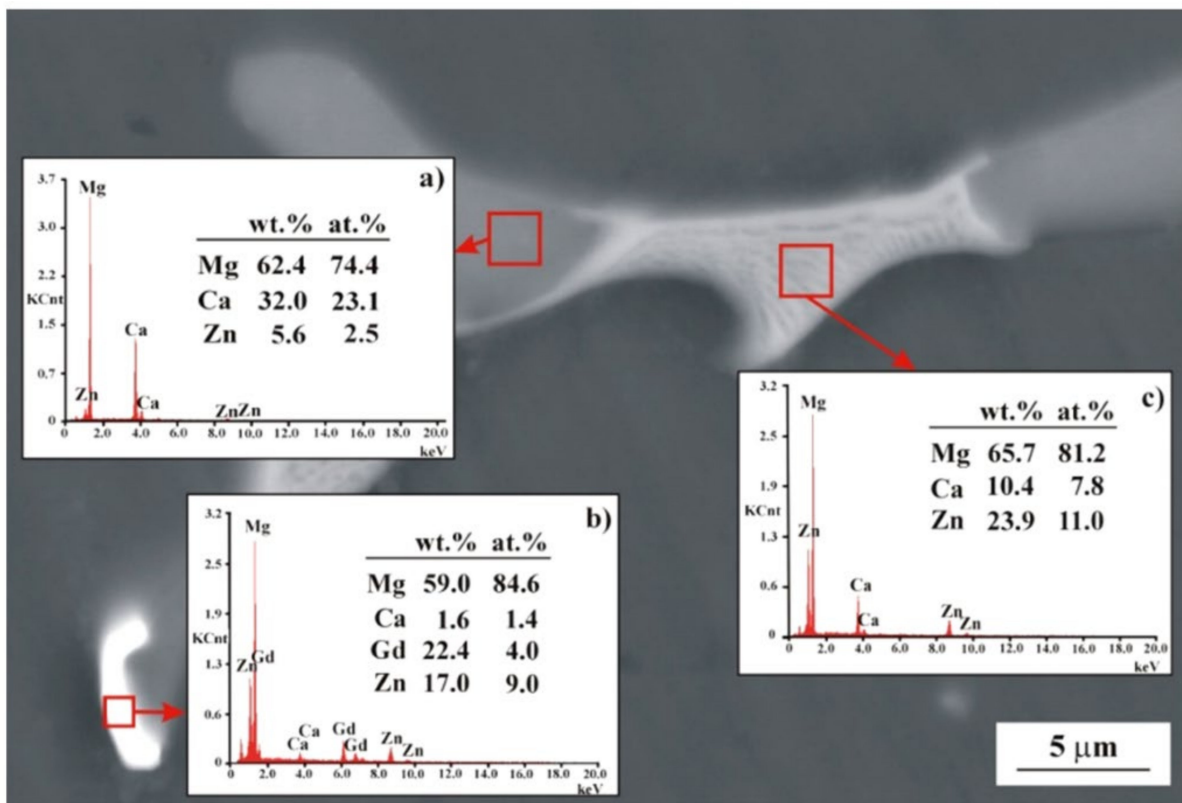


Figure 14. SEM image of MgCa<sub>3</sub>Zn<sub>1</sub>Gd<sub>2</sub> alloy with EDS spectra (a–c) from selected areas [138].

The calcium in magnesium is highly suitable for refinement in grain size of the alloy and significantly improves the resistance to corrosion and compressive and tensile strength of Mg alloys [13]. Therefore, the addition of REE (rare earth elements) also results in further improvement in the mechanical properties of Mg–Ca alloys [74]. The alloying element yttrium in Mg–Ca alloy improved the resistance to corrosion and elongation to around 15.9% and formed a new Mg–1Ca–1Y alloy [68]. The mechanical properties of the Mg–Ca–Y–Zr alloy were also shown to be increased with the addition of yttrium [70]. The addition of yttrium improves ultimate tensile strength to 19 MPa, yield strength to 120 MPa, and elongation to 8.3% in Mg–Ca–Y–Zr alloy [70].

### 3.4. Mg–RE Alloy

The strength and formability of the alloy are the two most important parameters that are concerned when using wrought Mg–RE alloys that enable its usage in various applications [50]. One research study suggested that the addition of rare earth elements improves the formability of the alloy along with the reduction in the texture of the alloy [2]. Irrespective of formability and strength, Mg-based alloys are strengthened via precipitation subtending to the addition of rare earth elements [74]. The rare earth elements that are most frequently used with Mg alloys are lanthanum, gadolinium, yttrium, holmium, erbium, ytterbium, cerium, and neodymium [2]. The research study suggested that the Mg–Gd–Y–Zn–Zr alloy is the strongest magnesium extrusion alloy having a tensile yield strength of the alloy around 480 MPa [91]. The addition of a higher concentration of rare earth elements in magnesium alloys are often not suitable to be employed in biomedical application and lowers the compressive strength of the alloy [50]. The precipitation quality is directly dependent on age-hardening and assessed by the size, orientation, density, morphology, and structure of the magnesium alloy matrix [111]. A research study suggested that processing methods and alloying elements affect the overall mechanical properties of magnesium and its alloys. The magnesium casting alloy involves large amounts of Gd (gadolinium), having a higher value of ultimate tensile strength of more than 350 MPa [50].

The newly created Mg-1.5Y-1.2Zn-0.44Zr alloys are biodegradable metallic compounds. According to the microstructure observations, the matrix  $\alpha$ -Mg phases and the  $Mg_{12}ZnY$  secondary phases make up the majority of the Mg-1.5Y-1.2Zn-0.44Zr alloys (LPS structure). Hot extrusion greatly improves the mechanical characteristics and biodegradation resistance of alloys by significantly refining the grains and eliminating as-cast alloy defects [115]. The alloy's tensile strength and tensile yield strength are around 236 and 178 MPa, respectively, in the as-extruded condition, with an outstanding elongation of 28%. While this is happening, the compressive strength is around 471 MPa, and the bending strength is approximately 501 MPa [115]. The exceptional ductility of the hot-extruded alloys is further illustrated by the greater bending strength. According to the results of immersion tests and electrochemical analyses in the SBF, a protective film precipitated on the alloy's surface as the deterioration process progressed.  $Mg(OH)_2$  and hydroxyapatite (HA), which might boost osteoblast activity and encourage good biocompatibility, are present in the protective coating. The Mg-1.5Y-1.2Zn-0.44Zr alloys may be employed in biomedical applications because no significant cytotoxicity toward L-929 cells was found, and immersion extracts of alloy samples might increase cell proliferation over time in the cytotoxicity tests [115]. After soaking in the SBF solution for 240 h, the EDS results show that the hot-extruded alloy samples' surface degradation products were rich in O, Mg, P, and Ca, as shown in Figure 15a. Both the calcium and phosphorus parts come from the SBF. The alloy samples submerged in the SBF for 360 h were examined by XRD to ascertain the phase composition of the degradation products, as shown in Figure 15b. The differing state alloy samples' predominant degradation products are  $Mg(OH)_2$  and hydroxyapatite (HA), according to the XRD patterns. Furthermore, due to the as-extruded alloy's better deterioration resistance in the SBF, the peak intensities of these two components in the spectra are substantially lower than those of the as-cast and heat-treated ones. Figure 15c depicts the polarization behavior of the Mg-1.5Y-1.2Zn-0.44Zr alloys in the SBF solution as-cast, after heat treatment, and after extrusion. The findings indicate that hot extrusion effectively enhances corrosion resistance because it changes the corrosion potential of the as-cast Mg-1.5Y-1.2Zn-0.44Zr-based alloy positively and decreases the corrosion current [115]. The electrochemical impedance spectroscopy (EIS) results of the Mg-1.5Y-1.2Zn-0.44Zr alloys in the SBF as cast, heat treated, and extruded are shown in Figure 15d in the form of a Nyquist plot, which shows that all of the curves exhibit a single capacitive loop at all frequencies. The capacitive semi-diameter circles and deterioration rate are strongly correlated. Their EIS spectra, with the exception of diameter, are comparable, indicating that the corrosion mechanism is the same, but the pace of deterioration is different. The widths of the capacitive loops in the various state alloys are nearly identical, but they become larger following heat treatment and hot extrusion operations. The alloy that is extruded, as expected, yields the largest diameter, indicating that it has the best corrosion resistance. Figure 15e depicts the EDS image of the secondary phase present in the alloy sample and Figure 15f represents the mechanical characteristics of the as-cast, as-heat treated, and hot-extruded alloy [115].

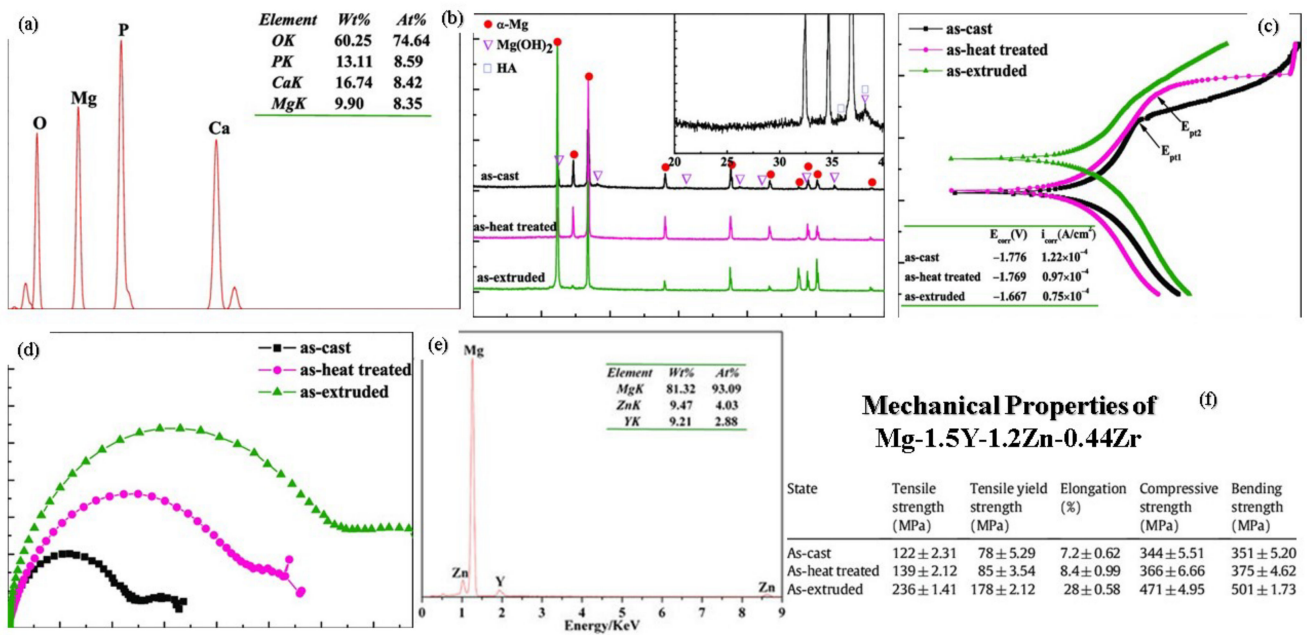


**Figure 15.** (a) EDS spectrum of the hot-extruded Mg-1.5Y-1.2Zn-0.44Zr alloy after soaking in the SBF (b) XRD image of the as-cast, as-heat treated, and as-extruded Mg-1.5Y-1.2Zn-0.44Zr alloy after being dipped in the SBF (c) Potentiodynamic polarization curves of the as-cast, as-heat treated and as-extruded Mg-1.5Y-1.2Zn-0.44Zr alloy samples in the SBF (d) Nyquist plots of the as-cast, heat treated, and extruded Mg-1.5Y-1.2Zn-0.44Zr alloys in the SBF (e) EDS spectrum from the secondary phase of alloy (f) Mechanical properties of the as-cast, heat treated, and extruded Mg-1.5Y-1.2Zn-0.44Zr alloys [115].

### Mg-RE-Zn Alloys

The Mg-10Y-2Zn alloy entails a high value of ultimate tensile strength (520 MPa), but the increase in the quantity of zinc to a smaller amount in magnesium alloy (Mg-6.7Y-2.5 Zn) leads to the further improvement in the ultimate tensile strength of the alloy (610 MPa); hence, Mg-6.7Y-2.5Zn alloy composition is regarded as the strongest alloy due to the higher elastic limit of Mg-6.7Y-2.5Zn as compared to titanium alloys (Ti-6Al-4V) and aluminum alloys (7075) [50]. Small grain refinement was observed with a diametrical range of 100–200 nm in the microstructural of Mg-Y-Zn alloy along with a depiction of uniform distribution of LPSO phase (Long Period Ordered Stacking) with a particle size of around 7nm along with the magnesium matrix [50]. The research study suggested that the most abundant LPSO phases were observed in Mg-Y-Zn alloy around 14H and 18R, which is resembled by the  $\gamma^j$  phase (disordered hexagonal structure) that adheres similarly to the matrix of magnesium [74]. The SEM depicted the similarity in the LPSO structures (18R and 14H) and the  $\gamma^j$  phase of the Mg-8Y-2Zn-0.6Zr alloy, but the research trend suggested that the Mg-6.7Y-2.5Zn alloy had insufficiency to yield around 610 MPa strength under hot extrusion other than producing 450 MPa yield strength [50]. The extrusion of Mg-Y-Zn alloys produced a yield strength of around 400 MPa, showing that the yield strength of the alloy is not influenced by the LPSO phase [139]. The LPSO particles generally reside around the grain boundary of magnesium-based alloys and will not dissolve in the Mg-matrix during the treatment of the alloy solution [140]. The researchers identified that the average particle size of magnesium in the Mg-Zn-Ca-Zr, Mg-Al-Ca, Mg-Y-Zn, or Mg-Zn-RE-Zr alloys was found to be few microns, as observed in the extruded state; as a result, a reduction in ductility was observed, that predicted the existence of the LPSO phase [50].

### 3.5. WE System Alloys

The addition of the yttrium element in magnesium significantly affects the strength and resistance to corrosion when employed in biodegradable applications [68]. The 4 wt.% of yttrium in WE43 alloy offers a reduction in resistance to corrosion of WE43 alloy [70]. The high concentration of yttrium in the WE43 alloy retards the corrosion growth and provided the uniform dispersion of powder in the WE43 alloy [71]. One research study suggested that WE43 alloy is effectively used for biomedical applications, having preferred biodegradable, biocompatible, and bioactive implant materials [71]. To analyze the in vitro corrosion rate, WE43 in SBF (simulated body fluid) shows the reduction in degradation rate due to the deposition of corrosion products over the surface of WE43 alloy [124]. Another research study suggested the formation of  $Y_2O_3$  oxide over the surface of WE43 alloy resembling high resistance to corrosion [120–123].

The phosphate-buffered saline (PBS) solution entails the reduction in corrosion rate for WE43 alloy [126]. Along with the reduction in corrosion rate, an increase in yield strength (190 MPa), ultimate strength (282 MPa), and elongation (37%) were observed [124]. Liu et al. investigated the mechanical characteristics of the WE43 alloy that show a reduction in grain size along the boundary and enhancement in the tensile strength (256 MPa) of the WE43 alloy [50]. One researcher compared the corrosion fatigue behavior of WE43 and AZ91D alloy and observed higher fatigue in WE43 extrusion than in AZ91D alloy [141–144]. Another study suggested that EW62 alloy (Mg-6% Nd-2% Y-0.5% Zr) is also effective for biomedical implantation, which had been investigated in SBF (simulated body fluid) for stress corrosion cracking and observed a lower corrosion rate [145].

A polymer that has high electrical conductivity and biocompatibility is polypyrrole (PPy) [146]. Recently, this has been utilized in biomedical applications such as the construction of artificial muscles, biosensors, the regulated release of medications, and neural recording stimulation of nerve regeneration [146,147]. In m-SBF (modified simulated body fluid) solution, the effect of Polypyrrole (PPy) coating on WE43 alloy against corrosion was investigated and produced a protective covering after being submerged for 24 h [118] slowed down the WE43 magnesium alloy's rate of corrosion [147]. Phosphate treatment is another effective way to improve the biocompatibility and corrosion resistance of WE43 alloys. In comparison to the uncoated alloys (more than 4ml per  $cm^2$  per day), the immersion test of phosphate-coated WE43 alloys revealed decreased hydrogen evolution (1 ml per  $cm^2$  per day) [130]. Additionally, the coated WE43 alloy outperformed the uncoated ones in terms of the vitality of the L-929 cell (96.21%). The stress corrosion cracking of magnesium alloy EW62 (Mg-6% Nd-2% Y-0.5% Zr) was studied in simulated fluids that suggested that the EW62 that solidifies quickly is a more biodegradable implant [131].

### 3.6. Mg-Li Alloys

The presence of lithium in Mg-Li alloy makes it a lightweight alloy due to a density of 0.533 g/cc [39]. The alloy with a lithium concentration of more than 11 wt.% indicated the presence of a single  $\beta$ -Li phase [40]. The research study suggested that the higher content of lithium in magnesium decreases the density of the alloy [40]. The binary Mg-Li alloy delivers a significant variation in ductility and depicted that the  $\alpha$ -Mg phase has low ductility and the  $\beta$ -Li phase has higher ductility [115–117]. Other than that, the increase in ductility is observed with the reduction in strength of the  $\beta$ -Li phase [115]. The Mg-Li alloy was alloyed with zinc and aluminum in order to improve the strength of the alloy [19–21]. The various intermetallic compounds that are formed via Zn and Al are Mg-Li-Zn, Mg-Li-2Al, and Mg-Li-2Zn, leading to an improvement in the mechanical properties of the alloy while having no drastic change in their corrosion resistance [39]. The presence of rare earth elements in Mg-Li alloy also improves the yield and tensile strength of the alloy along with the formation of secondary phase particles depicted in the extrusion process [74]. The LPFO phase in the second phase particle indicates the origin of reinforcement [117–119]. The Mg-5Li-3Al-2Zn-1.5Cu alloy among all the Mg-Li alloys indicated the highest yield strength of the alloy due to the precipitation of the Al-Cu phase [115]. The research study suggested

that the Mg-Li alloy is effective in biomedical implantation especially LAE442 (Mg-4 wt.%Li-3.6 wt.%Al-2.4 wt.%RE) [39]. The comparative study of LAE442 and AZ91D (Mg-9Al-1 Zn) alloy was subjected to in vitro and in vivo tests and recorded higher corrosion resistance in AZ91D than LAE442, but in vivo tests suggested higher corrosion resistance in LAE442 compared to AZ91D [115–117]. Table 6 depicted the comparative study of the influence of alloying elements on Mg-based alloy. The deformation twins inside the swaged samples are depicted in bright-field TEM images in Figure 16a–c, along with the associated SAED patterns close to the {1120} zone axis [148]. The twins' approximate placements are shown by the yellow dashed lines. Further straining caused localized stresses to form at the tips of certain primary twins, which aided in the formation of new twins. As a result, secondary twinning caused the grain to reorient itself, which may account for the production of LGBs with distinctive misorientation angles that were extensively seen in swaged samples. As seen in Figure 16d, a {1011} twin observed has a large density of parallel SFs lying on the basal plane. A clue pointing to basal-plane SFs is the streak reflections in the fast Fourier transform (FFT) pattern depicted in Figure 16d. Additionally, in Figure 16e, some SF segments are linked to the LGB in a well-aligned fashion [148]. The associated inverse Fast Fourier transform (IFFT) image reveals a variety of misfit dislocations. The core of this misfit dislocation, which is clearly visible in the insert IFFT image, is situated towards the end of the additional halfplane, which shows that these basal SFs are of the I1 type. According to the data in Figure 16f, the twin and SF average spacing values in the swaged sample are 289 and 11 nm, respectively. The atomic-scale structure of SFs was elucidated by aberration-corrected TEM to examine the dislocation interactions with SFs depicted in Figure 16g–i. Geometric phase analysis (GPA) of the HRTEM picture is used to first define the local displacement variations along SFs, which can reflect the strain distribution depicted in Figure 16h. The biggest dilatation (light-red color zone), as determined by quantitative GPA measurements, is linked to misfit dislocation. Dislocation core positions derived from this map are congruent with those shown in Figure 16g. The highest strain values were found close to the SFs' interface, which suggests that SFs on basal planes should have a similar impact to that of deformation twins in slowing dislocation migration [148].

**Table 6.** Comparative study of the influence of alloying elements on Mg-based alloy.

S.NO	Alloy	Researcher	Conclusion	References
1	Mg-Ca alloy	Li et al.	Ca concentrations between 1 and 20 wt.% to examine its biodegradability in bone. High Ca-concentration alloys, such as 5, 10, and 20 wt.% Ca were discovered to be brittle. By adjusting the Ca percentage, the mechanical characteristics and biocorrosion behavior of the Mg-Ca alloy can be improved. For as-cast Mg-Ca alloy samples, the YS, UTS, and elongation declined as the Ca concentration increased. The findings of the cytocompatibility evaluation showed that Mg-1Ca alloy does not cause cell toxicity.	[69]
2	Mg-Ca alloy	Rad et al.	Due to its great corrosion resistance, the Mg-0.5Ca alloy is a good choice for biodegradable implants.	[70]
3	Mg-Nd alloy	Seitz et al.	In low-loaded tissues, Nd can be used as a suitable alloying element for resorbable applications.	[71]
4	Mg-alloy (LANd442) (90 wt.% Mg, 4 wt.% Li, 4 wt.% Al, and 2 wt.% Nd)	Hampp et al.	LANd442 Mg alloy resulted in significant non-inflammatory bone remodeling activities, with new bone formation primarily occurring in the periosteal region. LANd442 might not be the best degradable implant material for applications involving cortical bone.	[73]

Table 6. Cont.

S.NO	Alloy	Researcher	Conclusion	References
5	Mg-Sn alloy	Bornapour et al.	After being submerged in SBF, a Sr-HAp layer formed on the surface of the binary Mg-Sr alloy. Additionally, this surface layer increased corrosion resistance.	[74]
6	Mg-Sr alloy	Nam et al.	Sr addition to Mg-5Al alloy had a considerable impact on the surface film, corrosion resistance, and grain boundaries. The development of the Mg <sub>17</sub> Al <sub>12</sub> phase at the grain boundaries prevented the precipitation of the Mg-Sr and Al-Sr phases. Additionally, Sr addition helped the surface's Al(OH) <sub>3</sub> protective coating to develop.	[75]
7	Mg-Zr alloy	Ramsden et al.	By adding Zr, Mg's grain size is reduced, improving the material's ductility, smoothing out the grain boundaries, and increasing corrosion resistance.	[90]
8	Mg-Sr alloy	Ai et al.	Sr refines the grain size in Mg alloys and has a high Mg alloying efficiency. Sr promotes biocompatibility, bone growth, and compressive strength. Sr concentrations beyond 2% in Mg-Zr-Sr alloys cause the intermetallic phase Mg <sub>17</sub> Sr <sub>2</sub> to precipitate at the grain boundary, which lowers corrosion resistance.	[95]
9	Mg-Zn-Ca alloy	Yadong et al.	The as-cast Mg-2Zn-0.5Ca alloy has the maximum UTS and elongation.	[96]
10	Mg-Gd-Ca-Zr	Shi et al.	The YS and compressive strength were enhanced with the addition of Ca, while the ductility decreased. Ca and Zr contributed to the alloy's improved mechanical performance for orthopedic applications.	[98]
11	Mg-3Sn-0.5Mn alloy	Zhen et al.	WE43 and AZ31 Mg alloys and Mg-3Sn-0.5Mn alloy had comparable UTS but were more ductile.	[99]
12	WE alloy	Wan et al.	WE alloy, Y (2.5 wt.% to 7.5 wt.%), and Nd (1–4.2 wt.%) content led to a decrease in ductility while increasing strength. Due to its low ductility, the alloy is more suitable for orthopedic implants than cardiovascular purposes.	[96]

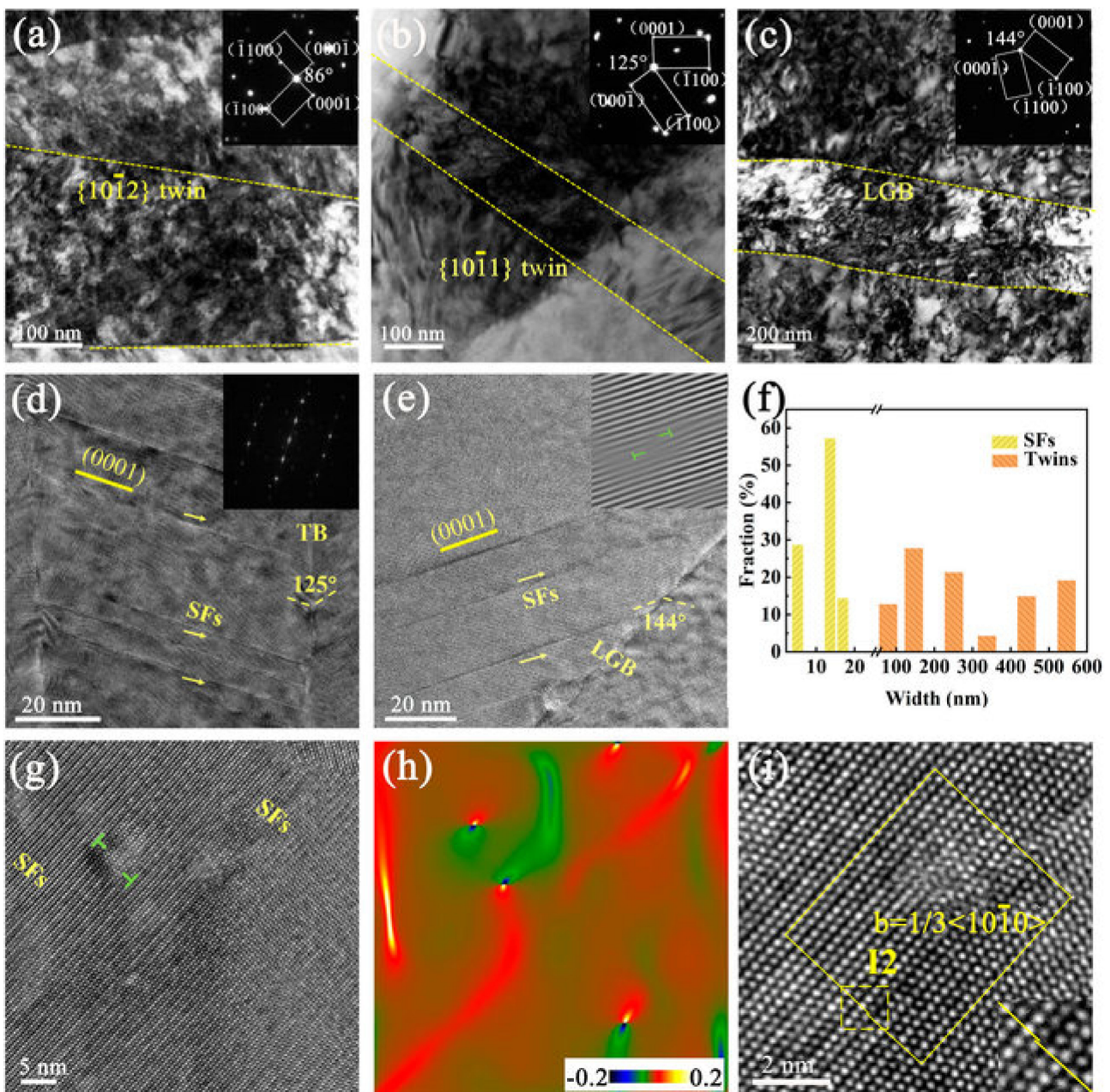


**Figure 16.** Twinning and SFs strengthening mechanisms were revealed by (HR)TEM. (a–c) Less-magnified TEM images and corresponding SAED patterns of lamellae structures in the Rotary swaging-processed Mg-Li alloy. (d) HRTEM image and corresponding FFT showing SFs in a {1011} twin. (e) HRTEM image and corresponding inverse Fast Fourier transform (IFFT) image of SFs in a lamellar grain. (f) The variation of width for twins and SFs. (g,h) Atomic-scale TEM images of SFs and corresponding GPA analysis. (i) HRTEM image showing an I2 fault bounded by  $1/3 \langle 10\bar{1}1 \rangle$  Shockley partials [148].

#### 4. Conclusions, Outlooks, and Future Aspects

Magnesium has a propensity to combine with other elements to produce alloys. Depending on how many alloying elements are added to magnesium, it can produce binary, ternary, or quaternary alloys. Mg-Ca, Mg-Al, Mg-Zn, Mg-RE, Mg-Li, and other significant alloys are a few examples. Depending on the manufacturing processes, the alloys are either cast alloys or extruded alloys when additional operations such as extrusion are performed. The literature on several kinds of magnesium alloys and their behavioral traits has been

compiled and thoroughly discussed. It should be noted that extruded alloys have higher mechanical characteristics than cast magnesium alloys, such as yield strength, ultimate tensile strength, or elongation due to the refined grains and produced homogenous microstructure. The attention has shifted to the development of Mg-RE alloys and Mg-Li alloys for biomedical applications due to their better characteristics. The uses of Mg-RE alloys in bioimplants have greatly increased as a result of their remarkable bio-functionality and biocompatibility. Several strategies have been used to overcome the problems of corrosion and the poor yield strength of pure magnesium, including the development of composites with suitable bioactive reinforcements, alloying, or surface modifications. Modern techniques were created to slow the pace of the corrosion of magnesium material and cure tissue damage without requiring additional surgery to remove the implanted material. The majority of researchers are working to produce implants for orthopedic applications and cardiovascular stents using biodegradable Mg-based materials. Due to the broad application of nanographene, recent developments in materials science and biomedical applications, such as scaffold, cancer nanotechnology, tissue manufacturing, drug delivery, and antimicrobial activities, have been incorporated. Eggshell has the potential to be exploited as efficient green reinforcing particles in the creation of Mg and Mg-Zr-based composites with better in vitro corrosion characteristics for biomedical applications.

Manganese is regarded as an essential element in the body that is required for a healthy bone–tissue framework. Aluminum enhances the susceptibility towards the stresses in corrosion cracking in alloys with the presence of  $\beta$ -phases in the composite. For biomedical implantation, 1 wt.% of calcium in Mg provides good accountability for biocompatibility. 0.1 wt.% of Mo in Mg alloy (AZ91E) at a micro-level improves the corrosion resistance. Holmium provides uniform dispersion and suitable compaction to the corrosion layer with the presence of a large amount of Al in Mg. The reduction in corrosion rate is observed at 2 to 3 wt.% of erbium in Mg-Al alloy. Cerium improves the corrosion rate in binary Mg-Ce alloy with the presence of the  $Mg_{12}Ce$  phase which improves the cathodic reaction rate. The increased corrosion resistance of Mg alloy (AZ91) is observed at 0.5 wt.% of lanthanum. Neodymium provides the protective oxides layer over the Mg-Al alloy surface comprising of Mg and rare earth elements which improves the resistance to corrosion. Strontium is regarded as a bone-seeking element that improves the remodeling and regeneration of injured/damaged bone and bone formation. Sr promotes biocompatibility, bone growth, and compressive strength, while 0.8 wt.% of yttrium in Mg alloy (AZ91) improves the corrosion resistance properties. Silver in Mg alloy (AZ91) improves the hardness of the alloy without affecting its resistance to corrosion. ZEK100, which is initially stable and degrades at a positive rate, is ideal for use in biodegradable implants. Mg-0.5Ca alloy is a good choice for biodegradable implants. Ca and Zr are most suitable for grain refining and contributed to the alloy's improved mechanical performance for orthopedic applications. The addition of a higher concentration of rare earth elements in magnesium alloys are often not suitable to be employed in biomedical applications as they lower the compressive strength of the alloy. WE43 alloy is effectively used for biomedical applications, having preferred biodegradable, biocompatible, and bioactive implant materials. EW62 alloy (Mg-6% Nd-2% Y-0.5% Zr) is also effective for biomedical implantation, having a lower corrosion rate.

Biodegradable magnesium alloys and implants constructed by them have been shown or anticipated to promote bone tissue regeneration, as well as have additional benefits in a variety of medicinal applications. However, before biodegradable magnesium alloys may be used in clinical settings, some processes must be developed to meet the needs of medical applications. The alloys' design and manufacture must, above all, meet the demands of the medical industry in terms of biocompatibility and mechanical integrity. The corrosion control strategy for magnesium alloys in medical applications, as one of the most significant procedures, should be created for the individual implants. Aside from resistance to corrosion, biocompatibility, high cell adhesion, wear resistance, and homogeneous surface morphology, the coverings should have a few more special features

for the implants. Some basic scientific problems about the coverings themselves, such as the degradation process of magnesium alloys, the biological characteristics and bio-absorbable routes of trace elements, or the bio-safety of Mg alloy implants after breakdown, require further fundamental investigation. In order to address load-bearing zone fractures, future research must focus on the development of alloys with a low degradation rate and improved mechanical strength. Additionally, it is necessary to look for new alloying components to improve the alloys' biocompatibility. If researchers are able to more closely match the clinical requirements with the bio-functional characteristics of each Mg-based alloy, new designs for orthopedic implants, particularly for foot and ankle surgery, may be built. In addition, Mg-based alloys have a huge potential to be used in the regenerative medicine field, due to the osteogenic properties of magnesium and its potential use for osseous defects caused by degenerative diseases.

**Author Contributions:** Conceptualization, S.K.S., K.K.S. and C.P.; methodology, K.A.M.; writing—original draft preparation, S.K.S. and K.K.S.; writing—review and editing, V.M., D.B., C.P. and S.D. All authors have read and agreed to the published version of the manuscript.

**Funding:** The research is partially funded by the Ministry of Science and Higher Education of the Russian Federation under the strategic academic leadership program 'Priority 2030' (Agreement 075-15-2021-1333 dated 30 September 2021).

**Institutional Review Board Statement:** Not applicable.

**Informed Consent Statement:** Not applicable.

**Data Availability Statement:** Not applicable.

**Conflicts of Interest:** The authors declare no conflict of interest.

## References

1. Singh, H.; Singh, S.; Prakash, C. Current trends in biomaterials and bio-manufacturing. In *Biomanufacturing*; Springer: Cham, Switzerland, 2019; pp. 1–34.
2. Singh, H.; Prakash, C.; Singh, S. Plasma spray deposition of HA-TiO<sub>2</sub> on  $\beta$ -phase Ti-35Nb-7Ta-5Zr alloy for hip stem: Characterization of bio-mechanical properties, wettability, and wear resistance. *J. Bionic Eng.* **2020**, *17*, 1029–1044. [[CrossRef](#)]
3. Prakash, C.; Kansal, H.K.; Pabla, B.S.; Puri, S.; Aggarwal, A. Electric discharge machining—A potential choice for surface modification of metallic implants for orthopedic applications: A review. *Proc. Inst. Mech. Eng. Part B J. Eng. Manuf.* **2016**, *230*, 331–353. [[CrossRef](#)]
4. Prakash, C.; Singh, S.; Gupta, M.K.; Mia, M.; Królczyk, G.; Khanna, N. Synthesis, characterization, corrosion resistance and in-vitro bioactivity behavior of biodegradable Mg–Zn–Mn–(Si–HA) composite for orthopaedic applications. *Materials* **2018**, *11*, 1602. [[CrossRef](#)] [[PubMed](#)]
5. Arora, G.S.; Saxena, K.K.; Mohammed, K.A.; Prakash, C.; Dixit, S. Manufacturing Techniques for Mg-Based Metal Matrix Composite with Different Reinforcements. *Crystals* **2022**, *12*, 945. [[CrossRef](#)]
6. Prakash, C.; Singh, S.; Pabla, B.S.; Sidhu, S.S.; Uddin, M.S. Bio-inspired low elastic biodegradable Mg-Zn-Mn-Si-HA alloy fabricated by spark plasma sintering. *Mater. Manuf. Processes* **2019**, *34*, 357–368. [[CrossRef](#)]
7. Singh, B.P.; Singh, R.; Mehta, J.S.; Prakash, C. August. Fabrication of biodegradable low elastic porous Mg-Zn-Mn-HA alloy by spark plasma sintering for orthopaedic applications. In *IOP Conference Series Materials Science and Engineering*; IOP Publishing: Bristol, UK, 2017; Volume 225, p. 012050.
8. Prakash, C.; Singh, S.; Verma, K.; Sidhu, S.S.; Singh, S. Synthesis and characterization of Mg-Zn-Mn-HA composite by spark plasma sintering process for orthopedic applications. *Vacuum* **2018**, *155*, 578–584. [[CrossRef](#)]
9. Sharma, S.K.; Kodli, B.K.; Saxena, K.K. Micro Forming and its Applications: An Overview. *Key Eng. Mater.* **2022**, *924*, 73–91. [[CrossRef](#)]
10. Sharma, S.K.; Saxena, K.K.; Kumar, K.B.; Kumar, N. The effect of reinforcements on the mechanical properties of AZ31 composites prepared by powder metallurgy: An overview. *Mater. Today Proc.* **2022**, *56*, 2293–2299. [[CrossRef](#)]
11. Dutta, S.; Gupta, S.; Roy, M. Recent developments in magnesium metal–matrix composites for biomedical applications: A Review. *ACS Biomater. Sci. Eng.* **2020**, *6*, 4748–4773. [[CrossRef](#)]
12. Huynh, V.; Ngo, N.K.; Golden, T.D. Surface activation and pretreatments for biocompatible metals and alloys used in biomedical applications. *Int. J. Biomater.* **2019**, *2019*, 3806504. [[CrossRef](#)]
13. Zheng, Y.F.; Gu, X.N.; Witte, F. Biodegradable metals. *Mater. Sci. Eng. R Rep.* **2014**, *77*, 1–34. [[CrossRef](#)]
14. Li, Q.; Zhong, X.; Hu, J.; Kang, W. Preparation and corrosion resistance studies of zirconia coating on fluorinated AZ91D magnesium alloy. *Prog. Org. Coat.* **2008**, *63*, 222–227. [[CrossRef](#)]

15. Rojaee, R.; Fathi, M.; Raeissi, K. Controlling the degradation rate of AZ91 magnesium alloy via sol–gel derived nanostructured hydroxyapatite coating. *Mater. Sci. Eng. C* **2013**, *33*, 3817–3825. [[CrossRef](#)]
16. Bommala, V.K.; Krishna, M.G.; Rao, C.T. Magnesium matrix composites for biomedical applications: A review. *J. Magnes. Alloy* **2019**, *7*, 72–79. [[CrossRef](#)]
17. Pal, K.; Asthana, N.; Aljabali, A.A.; Bhardwaj, S.K.; Kralj, S.; Penkova, A.; Gomes de Souza, F. A critical review on multifunctional smart materials ‘nanographene’ emerging avenue: Nano-imaging and biosensor applications. *Crit. Rev. Solid State Mater. Sci.* **2021**, *5*, 1–17. [[CrossRef](#)]
18. Panda, P.; Pal, K.; Chakroborty, S. Smart advancements of key challenges in graphene-assembly glucose sensor technologies: A mini review. *Mater. Lett.* **2021**, *303*, 130508. [[CrossRef](#)]
19. Aljabali, A.A.; Al Zoubi, M.S.; Al-Batayneh, K.M.; Pardhi, D.M.; Dua, K.; Pal, K.; Tambuwala, M.M. Innovative Applications of Plant Viruses in Drug Targeting and Molecular Imaging—A Review. *Curr. Med. Imaging* **2021**, *17*, 491–506. [[CrossRef](#)]
20. Santhosh, S.K.; Sarojini, S.; Umesh, M. Anti-Biofilm Activities of Nanocomposites Current Scopes and Limitations. In *Bio-manufactured Nanomaterials*; Springer: Cham, Switzerland, 2021; pp. 83–94.
21. Jayasathyakawin, S.; Ravichandran, M.; Baskar, N.; Chairman, C.A.; Balasundaram, R. Magnesium matrix composite for biomedical applications through powder metallurgy—Review. *Mater. Today Proc.* **2020**, *27*, 736–741. [[CrossRef](#)]
22. Kabir, H.; Munir, K.; Wen, C.; Li, Y. Recent research and progress of biodegradable zinc alloys and composites for biomedical applications: Biomechanical and biocorrosion perspectives. *Bioact. Mater.* **2021**, *6*, 836–879. [[CrossRef](#)]
23. Hussein, M.A.; Azeem, M.A.; Kumar, A.M.; Emar, N.M. Processing and in vitro Corrosion Analysis of Sustainable and Economical Eggshell Reinforced Mg and Mg–Zr Matrix Composite for Biomedical Applications. *Mater. Today Commun.* **2022**, *32*, 103944. [[CrossRef](#)]
24. Asiya, S.I.; Pal, K.; Kralj, S.; El-Sayyad, G.S.; de Souza, F.G.; Narayanan, T. Sustainable preparation of gold nanoparticles via green chemistry approach for biogenic applications. *Mater. Today Chem.* **2020**, *17*, 100327.
25. Singh, G.; Singh, S.; Prakash, C.; Ramakrishna, S. On investigating the soda-lime shot blasting of AZ31 alloy: Effects on surface roughness, material removal rate, corrosion resistance, and bioactivity. *J. Magnes. Alloy* **2021**, *9*, 1272–1284. [[CrossRef](#)]
26. Prakash, C.; Singh, S.; Ramakrishna, S. Characterization of indigenously coated biodegradable magnesium alloy primed through novel additive manufacturing assisted investment casting. *Mater. Lett.* **2020**, *275*, 128137. [[CrossRef](#)]
27. Bauer, J.C.; Chen, X.; Liu, Q.; Phan, T.H.; Schaak, R.E. Converting nanocrystalline metals into alloys and intermetallic compounds for applications in catalysis. *J. Mater. Chem.* **2008**, *18*, 275–282. [[CrossRef](#)]
28. Karunakaran, R.; Ortgies, S.; Tamayol, A.; Bobaru, F.; Sealy, M.P. Additive manufacturing of magnesium alloys. *Bioact. Mater.* **2020**, *5*, 44–54. [[CrossRef](#)]
29. Chen, K.; Dai, J.; Zhang, X. Improvement of corrosion resistance of magnesium alloys for biomedical applications. *Corros. Rev.* **2015**, *33*, 101–117. [[CrossRef](#)]
30. Singh, A.J. Beryllium—The Extraordinary Metal. *Miner. Processing Extr. Metallurgy Rev.* **1994**, *13*, 177–192. [[CrossRef](#)]
31. Witte, F.; Hort, N.; Vogt, C.; Cohen, S.; Kainer, K.U.; Willumeit, R.; Feyerabend, F. Degradable biomaterials based on magnesium corrosion. *Curr. Opin. Solid State Mater. Sci.* **2008**, *12*, 63–72. [[CrossRef](#)]
32. Chawla, K.K. Metal matrix composites. In *Composite Materials*; Springer: New York, NY, USA, 2012; pp. 197–248.
33. Chen, Q.; Thouas, G.A. Metallic implant biomaterials. *Mater. Sci. Eng. R Rep.* **2015**, *87*, 1–57. [[CrossRef](#)]
34. Wan, Y.; Xiong, G.; Luo, H.; He, F.; Huang, Y.; Zhou, X. Preparation and characterization of a new biomedical magnesium–calcium alloy. *Mater. Des.* **2008**, *29*, 2034–2037. [[CrossRef](#)]
35. Moustafa, M.A.; Samuel, F.H.; Doty, H.W. Effect of solution heat treatment and additives on the microstructure of Al–Si (A413. 1) automotive alloys. *J. Mater. Sci.* **2003**, *38*, 4507–4522. [[CrossRef](#)]
36. Dahle, A.K.; Lee, Y.C.; Nave, M.D.; Schaffer, P.L.; StJohn, D.H. Development of the as-cast microstructure in magnesium–aluminium alloys. *J. Light Met.* **2001**, *1*, 61–72. [[CrossRef](#)]
37. Rosliza, R.; Nik, W.W.; Senin, H.B. The effect of inhibitor on the corrosion of aluminum alloys in acidic solutions. *Mater. Chem. Phys.* **2008**, *107*, 281–288. [[CrossRef](#)]
38. Xu, W.; Xin, Y.C.; Zhang, B.; Li, X.Y. Stress corrosion cracking resistant nanostructured Al–Mg alloy with low angle grain boundaries. *Acta Mater.* **2022**, *225*, 117607. [[CrossRef](#)]
39. Yan, X.; Wan, P.; Tan, L.; Zhao, M.; Shuai, C.; Yang, K. Influence of hybrid extrusion and solution treatment on the microstructure and degradation behavior of Mg–0.1 Cu alloy. *Mater. Sci. Eng. B* **2018**, *229*, 105–117. [[CrossRef](#)]
40. Ghali, E.; Dietzel, W.; Kainer, K.U. General and localized corrosion of magnesium alloys: A critical review. *J. Mater. Eng. Perform.* **2004**, *13*, 7–23. [[CrossRef](#)]
41. Ardakani, M.S.; Mostaed, E.; Sikora-Jasinska, M.; Kampe, S.L.; Drelich, J.W. The effects of alloying with Cu and Mn and thermal treatments on the mechanical instability of Zn–0.05 Mg alloy. *Mater. Sci. Eng. A* **2020**, *770*, 138529. [[CrossRef](#)]
42. Bakhsheshi-Rad, H.R.; Idris, M.H.; Abdul-Kadir, M.R.; Ourdjini, A.; Medraj, M.; Daroonparvar, M.; Hamzah, E. Mechanical and bio-corrosion properties of quaternary Mg–Ca–Mn–Zn alloys compared with binary Mg–Ca alloys. *Mater. Des.* **2014**, *53*, 283–292. [[CrossRef](#)]
43. Lin, T.W.; Huang, S.D. Direct and simultaneous determination of copper, chromium, aluminum, and manganese in urine with a multielement graphite furnace atomic absorption spectrometer. *Anal. Chem.* **2001**, *73*, 4319–4325. [[CrossRef](#)]

44. Milovanovic, P.; Vom Scheidt, A.; Mletzko, K.; Sarau, G.; Püschel, K.; Djuric, M.; Amling, M.; Christiansen, S.; Busse, B. Bone tissue aging affects mineralization of cement lines. *Bone* **2018**, *110*, 187–193. [[CrossRef](#)]
45. Palacios, C. The role of nutrients in bone health, from A to Z. *Crit. Rev. Food Sci. Nutr.* **2006**, *46*, 621–628. [[CrossRef](#)]
46. Sharma, S.K.; Saxena, K.K.; Kumar, N. Influence of SiC on the mechanical properties of aluminum-based metal-matrix composites obtained by stir casting. *Met. Sci. Heat Treatment of Metals* **2022**, *6*, 24–28.
47. Ungureanu, G.; Santos, S.; Boaventura, R.; Botelho, C. Arsenic and antimony in water and wastewater: Overview of removal techniques with special reference to latest advances in adsorption. *J. Environ. Manag.* **2015**, *151*, 326–342. [[CrossRef](#)]
48. Deng, M.; Wang, L.; Höche, D.; Lamaka, S.V.; Snihirova, D.; Jiang, P.; Zheludkevich, M.L. Corrosion and discharge properties of Ca/Ge micro-alloyed Mg anodes for primary aqueous Mg batteries. *Corros. Sci.* **2020**, *177*, 108958. [[CrossRef](#)]
49. Zheng, Q.; Li, J.; Yuan, W.; Liu, X.; Tan, L.; Zheng, Y.; Wu, S. Metal-organic frameworks incorporated polycaprolactone film for enhanced corrosion resistance and biocompatibility of Mg Alloy. *ACS Sustain. Chem. Eng.* **2019**, *7*, 18114–18124. [[CrossRef](#)]
50. Witte, F.; Feyerabend, F.; Maier, P.; Fischer, J.; Störmer, M.; Blawert, C.; Dietzel, W.; Hort, N. Biodegradable magnesium hydroxyapatite metal matrix composites. *Biomaterials* **2007**, *28*, 2163–2174. [[CrossRef](#)]
51. Liu, R.L.; Scully, J.R.; Williams, G.; Birbilis, N. Reducing the corrosion rate of magnesium via microalloying additions of group 14 and 15 elements. *Electrochim. Acta* **2018**, *260*, 184–195. [[CrossRef](#)]
52. Asl, K.M.; Tari, A.; Khomamizadeh, F. Effect of deep cryogenic treatment on microstructure, creep and wear behaviors of AZ91 magnesium alloy. *Mater. Sci. Eng. A* **2009**, *523*, 27–31. [[CrossRef](#)]
53. Lu, L.; Thong, K.K.; Gupta, M. Mg-based composite reinforced by Mg<sub>2</sub>Si. *Compos. Sci. Technol.* **2003**, *63*, 627–632. [[CrossRef](#)]
54. Czerwinski, F. Controlling the ignition and flammability of magnesium for aerospace applications. *Corros. Sci.* **2014**, *86*, 1–16. [[CrossRef](#)]
55. Rahmatabadi, D.; Ahmadi, M.; Pahlavani, M.; Hashemi, R. DIC-based experimental study of fracture toughness through R-curve tests in a multi-layered Al-Mg (LZ91) composite fabricated by ARB. *J. Alloys Compd.* **2021**, *883*, 160843. [[CrossRef](#)]
56. Wang, W.; Yeung, K.W. Plasma surface modifications of orthopedic biomaterials by the adoption of bioinorganic cations: A review. *Surf. Innov.* **2020**, *8*, 203–215. [[CrossRef](#)]
57. Gusieva, K.; Davies, C.H.J.; Scully, J.R.; Birbilis, N. Corrosion of magnesium alloys: The role of alloying. *Int. Mater. Rev.* **2015**, *60*, 169–194. [[CrossRef](#)]
58. Hou, X.; Qin, H.; Gao, H.; Mankoci, S.; Zhang, R.; Zhou, X.; Ye, C. A systematic study of mechanical properties, corrosion behavior, aafter ultrasonic nanocrystal surface modification. *Mater. Sci. Eng. C* **2017**, *78*, 1061–1071. [[CrossRef](#)] [[PubMed](#)]
59. Zhang, J.; Zhu, Y.; Zang, X.; Huan, Q.; Su, W.; Zhu, D.; Li, L. Nickel-decorated graphene nanoplates for enhanced H<sub>2</sub> sorption properties of magnesium hydride at moderate temperatures.nd AZ31B Mg alloy biocompatibility. *J. Mater. Chem. A* **2016**, *4*, 2560–2570. [[CrossRef](#)]
60. Niu, H.Y.; Deng, K.K.; Nie, K.B.; Cao, F.F.; Zhang, X.C.; Li, W.G. Microstructure, mechanical properties and corrosion properties of Mg-4Zn-xNi alloys for degradable fracturing ball applications. *J. Alloys Compd.* **2019**, *787*, 1290–1300. [[CrossRef](#)]
61. Peron, M.; Torgersen, J.; Berto, F. Mg and its alloys for biomedical applications: Exploring corrosion and its interplay with mechanical failure. *Metals* **2017**, *7*, 252. [[CrossRef](#)]
62. Rosalbino, F.; Carlini, R.; Soggia, F.; Zanichchi, G.; Scavino, G. Influence of rare earth metals addition on the corrosion behaviour of copper in alkaline environment. *Corros. Sci.* **2012**, *58*, 139–144. [[CrossRef](#)]
63. Shehzad, F.; Hussain, S.M.S.; Adewunmi, A.A.; Mahboob, A.; Murtaza, M.; Kamal, M.S. Magnetic surfactants: A review of recent progress in synthesis and applications. *Adv. Colloid Interface Sci.* **2021**, *293*, 102441. [[CrossRef](#)]
64. Rosalbino, F.; Angelini, E.; De Negri, S.; Saccone, A.; Delfino, S. Effect of erbium addition on the corrosion behaviour of Mg–Al alloys. *Intermetallics* **2005**, *13*, 55–60. [[CrossRef](#)]
65. Satya Prasad, S.V.; Prasad, S.B.; Verma, K.; Mishra, R.K.; Kumar, V.; Singh, S. The role and significance of Magnesium in modern day research-A review. *J. Magnes. Alloy.* **2022**, *10*, 1–61. [[CrossRef](#)]
66. Arrabal, R.; Matykina, E.; Pardo, A.; Merino, M.C.; Paucar, K.; Mohedano, M.; Casajús, P. Corrosion behaviour of AZ91D and AM50 magnesium alloys with Nd and Gd additions in humid environments. *Corros. Sci.* **2012**, *55*, 351–362. [[CrossRef](#)]
67. Zidane, N.; Albrimi, Y.A.; Addi, A.A.; Akbour, R.A.; Douch, J.; Nahle, A.; Hamdani, M. Effect of gadolinium content on the corrosion behavior of magnesium alloys in 1 wt.% NaCl solution. *Port. Electrochim. Acta* **2015**, *33*, 289–304. [[CrossRef](#)]
68. Pettersen, G.; Westengen, H.; Høier, R.; Lohne, O. Microstructure of a pressure die cast magnesium—4wt.% aluminium alloy modified with rare earth additions. *Mater. Sci. Eng. A* **1996**, *207*, 115–120. [[CrossRef](#)]
69. Moore, E.E.; Turchi, P.E.A.; Lordi, V.; Weiss, D.; Sims, Z.C.; Henderson, H.B.; Kesler, M.S.; Rios, O.; McCall, S.K.; Perron, A. Thermodynamic Modeling of the Al-Ce-Cu-Mg-Si System and Its Application to Aluminum-Cerium Alloy Design. *J. Phase Equilibria Diffus.* **2020**, *41*, 764–783. [[CrossRef](#)]
70. Medina, J.; Pérez, P.; Garcés, G.; Adeva, P. Effects of calcium, manganese and cerium-rich mischmetal additions on the mechanical properties of extruded Mg-Zn-Y alloy reinforced by quasicrystalline I-phase. *Mater. Charact.* **2017**, *129*, 195–206. [[CrossRef](#)]
71. Alibabaei, S.; Kasiri-Asgarani, M.; Bakhsheshi-Rad, H. Investigating the effect of solid solution treatment on the corrosion properties of biodegradable Mg-Zn-RE-xCa (x = 0 2019, 2.5) alloy. *J. Simul. Anal. Nov. Technol. Mech. Eng.* **2019**, *12*, 67–80.
72. Peron, M.; Berto, F.; Torgersen, J. *Magnesium and Its Alloys as Implant Materials: Corrosion, Mechanical and Biological Performances*; CRC Press: Boca Raton, FL, USA, 2020.

73. Rzychoń, T.; Kielbus, A.; Lityńska-Dobrzyńska, L. Microstructure, microstructural stability and mechanical properties of sand-cast Mg–4Al–4RE alloy. *Mater. Charact.* **2013**, *83*, 21–34. [[CrossRef](#)]
74. Zhang, X.; Wang, Z.; Zhou, Z.; Xu, J. Effects of cerium and lanthanum on the corrosion behavior of Al-3.0 wt.% Mg alloy. *J. Mater. Eng. Perform.* **2016**, *25*, 1122–1128. [[CrossRef](#)]
75. Birbilis, N.; Easton, M.A.; Sudholz, A.D.; Zhu, S.M.; Gibson, M.A. On the corrosion of binary magnesium-rare earth alloys. *Corros. Sci.* **2009**, *51*, 683–689. [[CrossRef](#)]
76. Willbold, E.; Gu, X.; Albert, D.; Kalla, K.; Bobe, K.; Brauneis, M.; Janning, C.; Nellesen, J.; Czayka, W.; Tillmann, W.; et al. Effect of the addition of low rare earth elements (lanthanum, neodymium, cerium) on the biodegradation and biocompatibility of magnesium. *Acta Biomater.* **2015**, *11*, 554–562. [[CrossRef](#)]
77. Dermience, M.; Lognay, G.; Mathieu, F.; Goyens, P. Effects of thirty elements on bone metabolism. *J. Trace Elem. Med. Biol.* **2015**, *32*, 86–106. [[CrossRef](#)]
78. Gu, X.N.; Xie, X.H.; Li, N.; Zheng, Y.F.; Qin, L.J.A.B. In vitro and in vivo studies on a Mg–Sr binary alloy system developed as a new kind of biodegradable metal. *Acta Biomater.* **2012**, *8*, 2360–2374. [[CrossRef](#)]
79. Polmear, I.J. Magnesium alloys and applications. *Mater. Sci. Technol.* **1994**, *10*, 1–16. [[CrossRef](#)]
80. Prasad, A.; Uggowitz, P.J.; Shi, Z.; Atrens, A. Production of high purity magnesium alloys by melt purification with Zr. *Adv. Eng. Mater.* **2012**, *14*, 477–490. [[CrossRef](#)]
81. Ouyang, L.Z.; Yang, X.S.; Zhu, M.; Liu, J.W.; Dong, H.W.; Sun, D.L.; Zou, J.; Yao, X.D. Enhanced hydrogen storage kinetics and stability by synergistic effects of in situ formed CeH<sub>2</sub>. 73 and Ni in CeH<sub>2</sub>. 73-MgH<sub>2</sub>-Ni nanocomposites. *J. Phys. Chem. C* **2014**, *15*, 7808–7820. [[CrossRef](#)]
82. Habibnejad-Korayem, M.; Mahmudi, R.; Poole, W.J. Enhanced properties of Mg-based nano-composites reinforced with Al<sub>2</sub>O<sub>3</sub> nano-particles. *Mater. Sci. Eng. A* **2009**, *519*, 198–203. [[CrossRef](#)]
83. Feyerabend, F.; Fischer, J.; Holtz, J.; Witte, F.; Willumeit, R.; Drücker, H.; Vogt, C.; Hort, N. Evaluation of short-term effects of rare earth and other elements used in magnesium alloys on primary cells and cell lines. *Acta Biomater.* **2010**, *6*, 1834–1842. [[CrossRef](#)]
84. Zhang, J.; Niu, X.; Qiu, X.; Liu, K.; Nan, C.; Tang, D.; Meng, J. Effect of yttrium-rich misch metal on the microstructures, mechanical properties and corrosion behavior of die cast AZ91 alloy. *J. Alloys Compd.* **2009**, *471*, 322–330. [[CrossRef](#)]
85. Jafari, H.; Rahimi, F.; Sheikhsofla, Z. In vitro corrosion behavior of Mg-5Zn alloy containing low Y contents. *Mater. Corros.* **2016**, *67*, 396–405. [[CrossRef](#)]
86. Mordike, B.L. Creep-resistant magnesium alloys. *Mater. Sci. Eng. A* **2002**, *324*, 103–112. [[CrossRef](#)]
87. Zhang, Y.; Gore, P.; Rong, W.; Wu, Y.; Yan, Y.; Zhang, R.; Birbilis, N. Quasi-in-situ STEM-EDS insight into the role of Ag in the corrosion behaviour of Mg-Gd-Zr alloys. *Corros. Sci.* **2018**, *136*, 106–118. [[CrossRef](#)]
88. Zhu, L.; Song, G. Improved corrosion resistance of AZ91D magnesium alloy by an aluminium-alloyed coating. *Surf. Coat. Technol.* **2006**, *200*, 2834–2840. [[CrossRef](#)]
89. Pan, H.; Ren, Y.; Fu, H.; Zhao, H.; Wang, L.; Meng, X.; Qin, G. Recent developments in rare-earth free wrought magnesium alloys having high strength: A review. *J. Alloys Compd.* **2016**, *663*, 321–331. [[CrossRef](#)]
90. Cao, X.J.; Jahazi, M.; Immarigeon, J.P.; Wallace, W. A review of laser welding techniques for magnesium alloys. *J. Mater. Processing Technol.* **2006**, *171*, 188–204. [[CrossRef](#)]
91. Agarwal, S.; Curtin, J.; Duffy, B.; Jaiswal, S. Biodegradable magnesium alloys for orthopaedic applications: A review on corrosion, biocompatibility and surface modifications. *Mater. Sci. Eng. C* **2016**, *68*, 948–963. [[CrossRef](#)]
92. Gialanella, S.; Malandrucolo, A. Alloys for aircraft structures. In *Aerospace Alloys*; Springer: Cham, Switzerland, 2020; pp. 41–127.
93. Sharma, S.K.; Saxena, K.K. Effects on microstructure and mechanical properties of AZ31 reinforced with CNT by powder metallurgy: An overview. *Mater. Today Proc.* **2022**, *56*, 2038–2042. [[CrossRef](#)]
94. Sharma, S.K.; Saxena, K.K. An outlook on the influence on mechanical properties of AZ31 reinforced with graphene nanoparticles using powder metallurgy technique for biomedical application. *Mater. Today Proc.* **2022**, *56*, 2278–2287. [[CrossRef](#)]
95. Li, L.; Li, D.; Zeng, X.; Luo, A.A.; Hu, B.; Sachdev, A.K.; Ding, W. Microstructural evolution of Mg-Al-Re alloy reinforced with alumina fibers. *J. Magnes. Alloy.* **2020**, *8*, 565–577. [[CrossRef](#)]
96. Yao, S.; Liu, S.; Zeng, G.; Li, X.; Lei, T.; Li, Y.; Du, Y. Effect of manganese on microstructure and corrosion behavior of the Mg-3Al alloys. *Metals* **2019**, *9*, 460. [[CrossRef](#)]
97. Chu, A.; Zhao, Y.; Ud-Din, R.; Hu, H.; Zhi, Q.; Wang, Z. Microstructure and properties of Mg-Al-Ca-Mn alloy with high Ca/Al ratio fabricated by hot extrusion. *Materials* **2021**, *14*, 5230. [[CrossRef](#)] [[PubMed](#)]
98. Kielbus, A.; Jarosz, R.; Gryc, A. Effect of modification on microstructure and properties of AZ91 magnesium alloy. *Crystals* **2020**, *10*, 536. [[CrossRef](#)]
99. Krawiec, H.; Stanek, S.; Vignal, V.; Lelito, J.; Suchy, J.S. The use of microcapillary techniques to study the corrosion resistance of AZ91 magnesium alloy at the microscale. *Corros. Sci.* **2011**, *53*, 3108–3113. [[CrossRef](#)]
100. Mert, F.; Blawert, C.; Kainer, K.U.; Hort, N. Influence of cerium additions on the corrosion behaviour of high pressure die cast AM50 alloy. *Corros. Sci.* **2012**, *65*, 145–151. [[CrossRef](#)]
101. StJohn, D.H.; Easton, M.A.; Qian, M.; Taylor, J.A. Grain refinement of magnesium alloys: A review of recent research, theoretical developments, and their application. *Metall. Mater. Trans. A* **2013**, *44*, 2935–2949. [[CrossRef](#)]
102. Manivasagam, T.G.; Kiraz, K.; Notten, P.H. Electrochemical and optical properties of magnesium-alloy hydrides reviewed. *Crystals* **2012**, *2*, 1410–1433. [[CrossRef](#)]

103. Akbaripannah, F.; Fereshteh-Saniee, F.; Mahmudi, R.; Kim, H.K. Microstructural homogeneity, texture, tensile and shear behavior of AM60 magnesium alloy produced by extrusion and equal channel angular pressing. *Mater. Des.* **2013**, *43*, 31–39. [[CrossRef](#)]
104. Sun, X.; Su, Y.; Huang, Y.; Chen, M.; Liu, D. Microstructure Evolution and Properties of  $\beta$ -TCP/Mg-Zn-Ca Biocomposite Processed by Hot Extrusion Combined with Multi-Pass ECAP. *Metals* **2022**, *12*, 685. [[CrossRef](#)]
105. Grimm, M.; Lohmüller, A.; Singer, R.F.; Virtanen, S. Influence of the microstructure on the corrosion behaviour of cast Mg-Al alloys. *Corros. Sci.* **2019**, *155*, 195–208. [[CrossRef](#)]
106. Ünlü, B.S. Investigation of tribological and mechanical properties Al<sub>2</sub>O<sub>3</sub>-SiC reinforced Al composites manufactured by casting or P/M method. *Mater. Des.* **2008**, *29*, 2002–2008. [[CrossRef](#)]
107. Chang, I.; Cai, Q. From simple binary to complex multicomponent eutectic alloys. *Prog. Mater. Sci.* **2022**, *123*, 100779. [[CrossRef](#)]
108. Predko, P.; Rajnovic, D.; Grilli, M.L.; Postolnyi, B.O.; Zemcenkovs, V.; Rijkuris, G.; Pole, E.; Lisnanskis, M. Promising Methods for Corrosion Protection of Magnesium Alloys in the Case of Mg-Al, Mg-Mn-Ce and Mg-Zn-Zr: A Recent Progress Review. *Metals* **2021**, *11*, 1133. [[CrossRef](#)]
109. Zhu, M.; Wang, H.; Ouyang, L.Z.; Zeng, M.Q. Composite structure and hydrogen storage properties in Mg-base alloys. *Int. J. Hydrogen Energy* **2006**, *31*, 251–257. [[CrossRef](#)]
110. Sandlöbes, S.; Friák, M.; Korte-Kerzel, S.; Pei, Z.; Neugebauer, J.; Raabe, D. A rare-earth free magnesium alloy with improved intrinsic ductility. *Sci. Rep.* **2017**, *7*, 1–8. [[CrossRef](#)]
111. Li, R.; Pan, F.; Jiang, B.; Dong, H.; Yang, Q. Effect of Li addition on the mechanical behavior and texture of the as-extruded AZ31 magnesium alloy. *Mater. Sci. Eng. A* **2013**, *562*, 33–38. [[CrossRef](#)]
112. You, S.; Huang, Y.; Kainer, K.U.; Hort, N. Recent research and developments on wrought magnesium alloys. *J. Magnes. Alloy.* **2017**, *5*, 239–253. [[CrossRef](#)]
113. Bae, G.T.; Bae, J.H.; Kang, D.H.; Lee, H.; Kim, N.J. Effect of Ca addition on microstructure of twin-roll cast AZ31 Mg alloy. *Met. Mater. Int.* **2009**, *15*, 1–5. [[CrossRef](#)]
114. Korgiopoulos, K.; Langelier, B.; Pekguleryuz, M. Mg<sub>17</sub>Al<sub>12</sub> phase refinement and the improved mechanical performance of Mg–6Al alloy with trace erbium addition. *Mater. Sci. Eng. A* **2021**, *812*, 141075. [[CrossRef](#)]
115. Fan, J.; Qiu, X.; Niu, X.; Tian, Z.; Sun, W.; Liu, X.; Meng, J. Microstructure, mechanical properties, in vitro degradation and cytotoxicity evaluations of Mg–1.5 Y–1.2 Zn–0.44 Zr alloys for biodegradable metallic implants. *Mater. Sci. Eng. C* **2013**, *33*, 2345–2352. [[CrossRef](#)]
116. Lee, C.J.; Huang, J.C.; Hsieh, P.J. Mg based nano-composites fabricated by friction stir processing. *Scr. Mater.* **2006**, *54*, 1415–1420. [[CrossRef](#)]
117. Go, J.; Jin, S.C.; Kim, H.; Yu, H.; Park, S.H. Novel Mg–Bi–Al alloy with extraordinary extrudability and high strength. *J. Alloys Compd.* **2020**, *843*, 156026. [[CrossRef](#)]
118. Liu, X.; Chen, X.; Li, J.; Liu, C.; Zhao, D.; Cheng, R.; Pan, F. Effect of micro-alloying Ca on microstructure, texture and mechanical properties of Mg–Zn–Y–Ce alloys. *Prog. Nat. Sci. Mater. Int.* **2020**, *30*, 213–220. [[CrossRef](#)]
119. Kumar, A.; Meenashisundaram, G.K.; Manakari, V.; Parande, G.; Gupta, M. Lanthanum effect on improving CTE, damping, hardness and tensile response of Mg–3Al alloy. *J. Alloys Compd.* **2017**, *695*, 3612–3620. [[CrossRef](#)]
120. Liu, J.; Bian, D.; Zheng, Y.; Chu, X.; Lin, Y.; Wang, M.; Lin, Z.; Li, M.; Zhang, Y.; Guan, S. Comparative in vitro study on binary Mg-RE (Sc, Y, La, Ce, Pr, Nd, Sm, Eu, Gd, Tb, Dy, Ho, Er, Tm, Yb and Lu) alloy systems. *Acta Biomater.* **2020**, *102*, 508–528. [[CrossRef](#)]
121. Tao, W.; Milin, Z.; Zhongyi, N.; Bin, L. Influence of rare earth elements on microstructure and mechanical properties of Mg-Li alloys. *J. Rare Earths* **2006**, *24*, 797–800. [[CrossRef](#)]
122. Wang, J.; Shi, N.; Wang, L.; Wu, Y.; Cao, Z.; Wang, L. Preparation and characterization of As-cast and hot-rolled Mg–3Al–0.5 Mn–0.5 Zn–1MM alloy. *Mater. Charact.* **2009**, *60*, 1507–1511. [[CrossRef](#)]
123. Jaiswal, S.; Kumar, R.M.; Gupta, P.; Kumaraswamy, M.; Roy, P.; Lahiri, D. Mechanical, corrosion and biocompatibility behaviour of Mg–3Zn–HA biodegradable composites for orthopaedic fixture accessories. *J. Mech. Behav. Biomed. Mater.* **2018**, *78*, 442–454. [[CrossRef](#)]
124. Zhang, X.; Chen, Y.; Hu, J. Recent advances in the development of aerospace materials. *Prog. Aerosp. Sci.* **2018**, *97*, 22–34. [[CrossRef](#)]
125. Du, Y.Z.; Qiao, X.G.; Zheng, M.Y.; Wu, K.; Xu, S.W. Development of high-strength, low-cost wrought Mg–2.5 mass% Zn alloy through micro-alloying with Ca and La. *Mater. Des.* **2015**, *85*, 549–557. [[CrossRef](#)]
126. Zeng, Z.; Stanford, N.; Davies, C.H.J.; Nie, J.F.; Birbilis, N. Magnesium extrusion alloys: A review of developments and prospects. *Int. Mater. Rev.* **2019**, *64*, 27–62. [[CrossRef](#)]
127. Peng, P.; Tang, A.; Wang, B.; Zhou, S.; She, J.; Zhang, J.; Pan, F. Achieving superior combination of yield strength and ductility in Mg–Mn–Al alloys via ultrafine grain structure. *J. Mater. Res. Technol.* **2021**, *15*, 1252–1265. [[CrossRef](#)]
128. Bi, J.; Lei, Z.; Chen, Y.; Chen, X.; Tian, Z.; Liang, J.; Qin, X.; Zhang, X. Densification, microstructure and mechanical properties of an Al–14.1 Mg–0.47 Si–0.31 Sc–0.17 Zr alloy printed by selective laser melting. *Mater. Sci. Eng. A* **2020**, *774*, 138931. [[CrossRef](#)]
129. Nie, J.F. Precipitation and hardening in magnesium alloys. *Metall. Mater. Trans. A* **2012**, *43*, 3891–3939. [[CrossRef](#)]
130. Yuan, B.; Li, G.; Guo, M.; Zhuang, L. Fast age-hardening response of Al–Mg–Si–Cu–Zn–Fe–Mn alloy via coupling control of quenching rate and pre-aging. *J. Mater. Res. Technol.* **2021**, *14*, 1518–1531. [[CrossRef](#)]

131. Garcés, G.; Máthis, K.; Medina, J.; Horváth, K.; Drozdenko, D.; Oñorbe, E.; Dobroň, P.; Pérez, P.; Klaus, M.; Adeva, P. Combination of in-situ diffraction experiments and acoustic emission testing to understand the compression behavior of Mg-Y-Zn alloys containing LPSO phase under different loading conditions. *Int. J. Plast.* **2018**, *106*, 107–128. [[CrossRef](#)]
132. Hänni, A.C.; Gunde, P.; Schinhammer, M.; Uggowitzner, P.J. On the biodegradation performance of an Mg-Y-RE alloy with various surface conditions in simulated body fluid. *Acta Biomater.* **2009**, *5*, 162–171. [[CrossRef](#)]
133. Czerwinski, F. The reactive element effect on high-temperature oxidation of magnesium. *Int. Mater. Rev.* **2015**, *60*, 264–296. [[CrossRef](#)]
134. Hiraga, K.; Ohsuna, T.; Yasuda, K.; Sugiyama, K. The structures of hexagonal phases in Mg-Zn-RE (RE = Sm and Gd) alloys. *Z. Krist.* **1998**, *213*, 537–543.
135. Sun, Y.; Zhang, B.; Wang, Y.; Geng, L.; Jiao, X. Preparation and characterization of a new biomedical Mg-Zn-Ca alloy. *Mater. Des.* **2012**, *34*, 58–64. [[CrossRef](#)]
136. Shi, L.; Huang, Y.; Yang, L.; Feyerabend, F.; Mendis, C.; Willumeit, R.; Kainer, K.U.; Hort, N. Mechanical properties and corrosion behavior of Mg-Gd-Ca-Zr alloys for medical applications. *J. Mech. Behav. Biomed. Mater.* **2015**, *47*, 38–48. [[CrossRef](#)]
137. Chaojie, C.; Cheng, L.; Tong, L.; Cai, Z.; Zhang, H. The effect of Gd and Zn additions on microstructures and mechanical properties of Mg-4Sm-3Nd-Zr alloy. *J. Alloys Compd.* **2017**, *706*, 526–537.
138. Kania, A.; Nowosielski, R.; Gawlas-Mucha, A.; Babilas, R. Mechanical and corrosion properties of Mg-based alloys with Gd addition. *Materials* **2019**, *12*, 1775. [[CrossRef](#)]
139. García-Galvan, F.R.; Fajardo, S.; Barranco, V.; Feliu, S. Experimental apparent stern–geary coefficients for AZ31B Mg alloy in physiological body fluids for accurate corrosion rate determination. *Metals* **2021**, *11*, 391. [[CrossRef](#)]
140. Chen, Y.; Xu, Z.; Smith, C.; Sankar, J. Recent advances on the development of magnesium alloys for biodegradable implants. *Acta Biomater.* **2014**, *10*, 4561–4573. [[CrossRef](#)]
141. Chen, L.; Sheng, Y.; Wang, X.; Zhao, X.; Liu, H.; Li, W. Effect of the microstructure and distribution of the second phase on the stress corrosion cracking of biomedical Mg-Zn-Zr-xSr alloys. *Materials* **2018**, *11*, 551. [[CrossRef](#)]
142. Mendis, C.L.; Bettles, C.J.; Gibson, M.A.; Gorse, S.; Hutchinson, C.R. Refinement of precipitate distributions in an age-hardenable Mg-Sn alloy through microalloying. *Philos. Mag. Lett.* **2006**, *86*, 443–456. [[CrossRef](#)]
143. Nene, S.S.; Kashyap, B.P.; Prabhu, N.; Estrin, Y.; Al-Samman, T. Microstructure refinement and its effect on specific strength and bio-corrosion resistance in ultralight Mg-4Li-1Ca (LC41) alloy by hot rolling. *J. Alloys Compd.* **2014**, *615*, 501–506. [[CrossRef](#)]
144. Kumari, S.; Nakum, B.; Bandhu, D.; Abhishek, K. Multi-Attribute Group Decision Making (MAGDM) Using Fuzzy Linguistic Modeling Integrated with the VIKOR Method for Car Purchasing Model. *Int. J. Decis. Support Syst. Technol. (IJDSST)* **2022**, *14*, 1–20. [[CrossRef](#)]
145. Sonia, P.; Kumari, S. Performance Evaluation of Multi-Fibre (Hybrid) Polymer Composite. *IOP Conf. Ser. Mater. Sci. Eng.* **2021**, *1116*, 012027. [[CrossRef](#)]
146. Ramanaviciene, A.; Kausaite, A.; Tautkus, S.; Ramanavicius, A. Biocompatibility of polypyrrole particles: An in-vivo study in mice. *J. Pharm. Pharmacol.* **2007**, *59*, 311–315. [[CrossRef](#)]
147. Tripathi, D.R.; Vachhani, K.H.; Bandhu, D.; Kumari, S.; Kumar, V.R.; Abhishek, K. Experimental investigation and optimization of abrasive waterjet machining parameters for GFRP composites using metaphor-less algorithms. *Mater. Manuf. Processes* **2021**, *36*, 803–813. [[CrossRef](#)]
148. Yang, Y.; Chen, X.; Nie, J.; Wei, K.; Mao, Q.; Lu, F.; Zhao, Y. Achieving ultra-strong Magnesium–lithium alloys by low-strain rotary swaging. *Mater. Res. Lett.* **2021**, *9*, 255–262. [[CrossRef](#)]